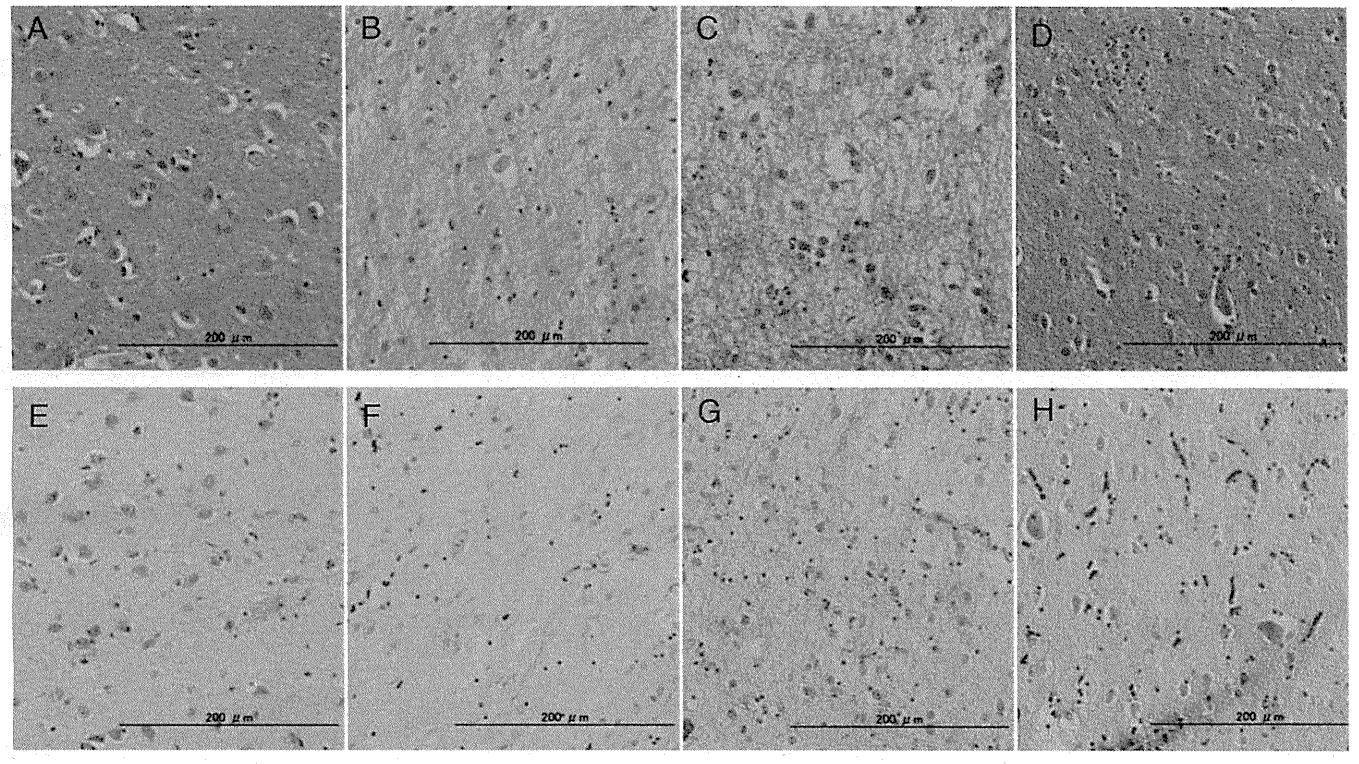

Fig. 3 Neuronal loss associated with glial proliferation in the caudate nucleus. Neither neuronal loss nor glial proliferation is noted in the normal control (A, E). Severe neuronal loss, remarkable glial proliferation, and tissue rarefaction are found in Case 1 (B, F) and Case 2 (C, G). Mild neuronal loss and glial proliferation are found, but no tissue rarefaction is seen in Case 3 (D, H). (A–D): HE stain; (E–H): KB stain. All scale bars = 200 μm.

ronal loss in the putamen was moderate in Case 1 (Fig. 4B,F) and Case 2 (Fig. 4C,G), but mild in Case 3 (Fig. 4D,H). Neuronal loss in the substantia nigra was moderate in Case 1 (Fig. 5B) and Case 2 (Fig. 5C), but mild in Case 3. The hippocampus showed severe neuronal loss in CA1, CA3 and the subiculum in Case 1, yet was preserved in Cases 2 and 3. The amygdaloid nucleus showed moderate neuronal loss in Case 1, with predominant involvement in the basolateral rather than the corticomedial area, but was preserved in Case 3 (Case 2 could not be examined). The cerebral cortex was relatively preserved in all cases. In the cerebellum, the cortex was almost normal, although a moderate loss of Purkinje cells was observed in Case 2.

Deposition of basophilic calcospherites

All three cases showed depositions of basophilic calcospherites, which were mainly found within the gray matter, such as the thalamus, caudate nucleus and putamen. While some calcospherites were located in perivascular sites as well as in blood vessel walls, most were not associated with blood vessels. Also, the calcospherites were not associated with gliosis or other pathological changes.

DISCUSSION

In the present study, we examined three cases of Nasu-Hakola disease in order to focus specifically on gray matter lesions. While genetic analysis was not performed, all the cases presented the typical pathology of the disease. Two types of neuropathology have been reported in Nasu-Hakola disease. One is characterized by marked demyelination, slight fibrillary gliosis and numerous sudanophilic deposits, a form of sudanophilic leukodystrophy. The other is characterized by marked fibrillary gliosis, slight demyelination, "dissociation glio-myelinique", and numerous spheroids in the cerebral white matter, a form of a sclerosing leukoencephalopathy.[10] The three cases addressed in this report belong to the latter type.

In addition to the characteristic degeneration of cerebral white matter, such as demyelination with conspicuous fibrillary gliosis and axonal changes, all three cases showed overt pathology in the gray matter. While the cerebral cortex was relatively preserved, neuronal loss and gliosis were observed in the thalamus (particularly in the dorsomedial nucleus and anterior nucleus), caudate nucleus, putamen and substantia nigra in all three cases. In addition, Case 1 showed neuronal loss and gliosis in the gray matter

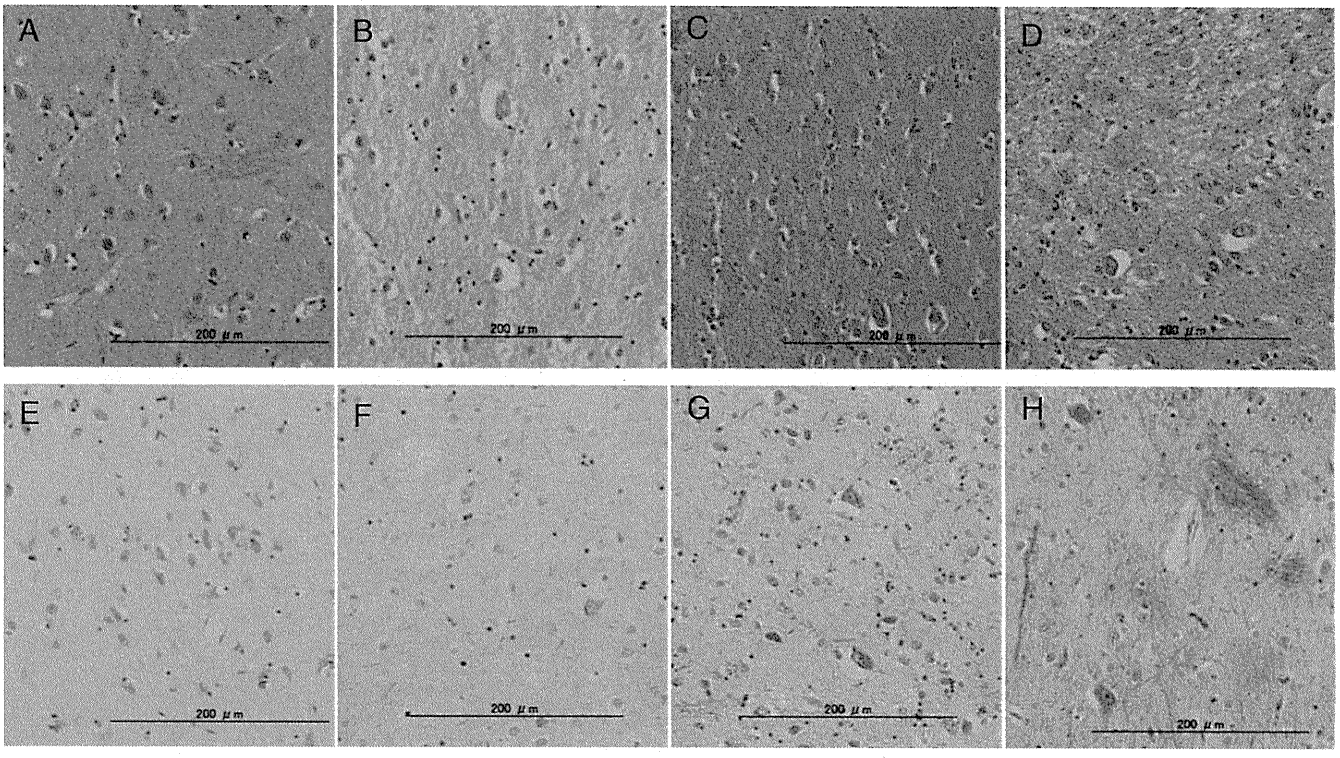

Fig. 4 Neuronal loss associated with glial proliferation in the putamen. Neither neuronal loss nor glial proliferation is noted in the normal control (A, E). Moderate neuronal loss and glial proliferation are found, but no tissue rarefaction is seen in Case 1 (B, F) and Case 2 (C, G). Mild neuronal loss and glial proliferation are found, but no tissue rarefaction is seen in Case 3 (D, H). (A–D): HE stain; (E–H): KB stain. All scale bars = 200 μm.

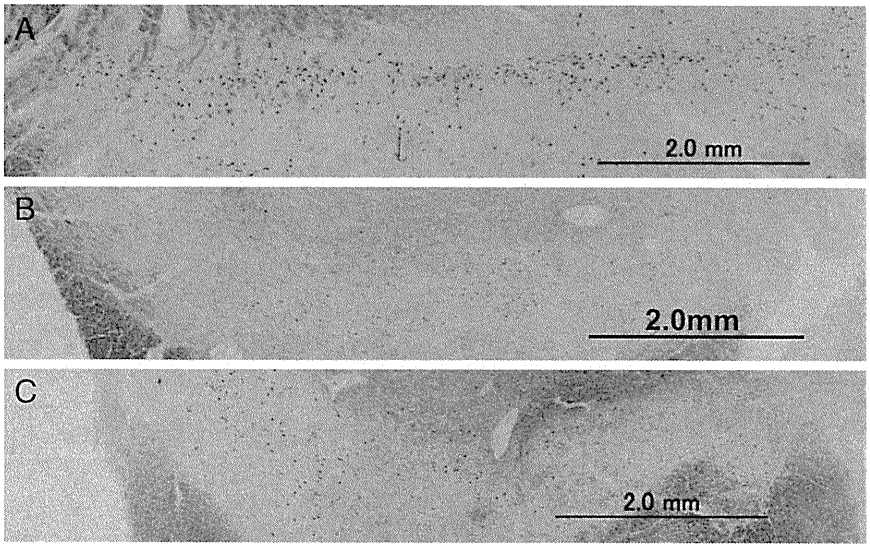

Fig. 5 The substantia nigra at low magnification. The number of neurons in Case 1 (B) and Case 2 (C) are moderately reduced, compared with the control (A). KB stain. All scale bars = 2.0 mm.

of the hippocampus and amygdala nucleus. Among the gray matter lesions, the thalamus was most severely affected. In Case 3, neuronal loss was generally mild, correlating with the shortest disease duration.

To date, gray matter lesions in Nasu-Hakola disease have been described in only a few reports.[11–14] Amano *et al.* reported a case showing neuronal loss in the thalamus (especially in the anterior and dorsomedial nucleus) and Purkinje cell layer, and astrocytosis in the putamen and globus pallidus. They reported that a long clinical course (33 years) and repeated episodes of convulsions might play a role in the lesions. Miyazu *et al.* also reported a case

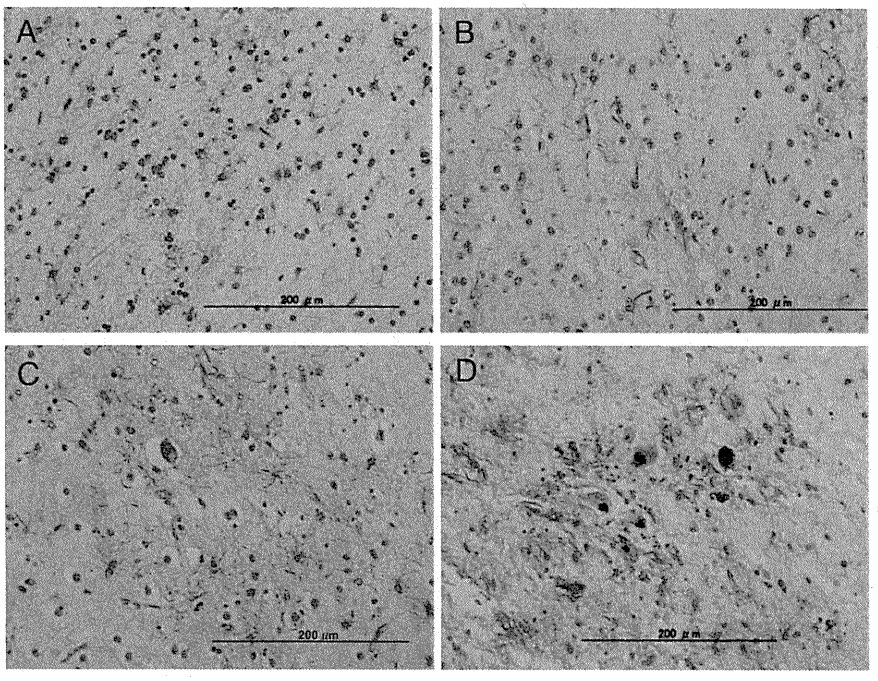

Fig. 6 Astrocytosis and gliosis in the thalamus (A), caudate nucleus (B), putamen (C) and substantia nigra (D). Holzer stain. All scale bars = 200 μm. (Case 1)

showing neuronal loss in the thalamus (particularly in the anterior, medial and pulvinar nucleus). Since this case experienced only a few episodes of convulsions and had a relatively short duration of disease, they considered the thalamic lesion to be a primary degeneration point. Paloneva *et al.* reported three cases showing neuronal loss in the thalamus, caudate nucleus and Purkinje cell layer, suggesting early basal ganglia involvement in this disease. The pathologies of the three cases described in this study corroborate the finding that neuronal loss is a constant feature of the thalamus and basal ganglia in Nasu-Hakola disease, while the neurons are relatively preserved in the cerebral cortex.

Although the precise pathomechanism underlying the gray matter lesions in Nasu-Hakola disease remains unknown, the following three factors are considered to be possible causes: dysfunction of the microglia, secondary changes due to axonal destruction, and convulsions. First, dysfunction of the microglia has been proposed to explain the CNS pathogenesis, since mutations in TREM2 and DAP12 have been identified as the primary causes of the disease.[5,6] Because microglia have the ability to phagocytose myelin,[15,16] the white matter may be severely damaged by abnormally activated microglia. Then the neuronal loss in the gray matter could be induced by defective functional activity in glial–neuronal interactions. Second, it is possible that the gray matter lesions are secondary changes due to axonal destruction in the white matter. In particular, the thalamus has many fiber connections with the frontal lobe through the white matter. While few reports focus on the gray matter lesions in other leukodystrophies, neuronal loss in the thalamus has frequently been reported.[17–19] For example, Tateishi *et al.* reported a case of adrenoleukodystrophy showing neuronal loss in the thalamus (particularly in the dorsomedial nucleus and anterior nucleus), the pontine nucleus, the inferior olivary nucleus and the cerebellar gray matter. Taken together with the distribution of white matter lesions, they concluded that the lesions were likely to be secondary changes in disruption of the thalamo-cortical, cerebro-ponto-cerebellar and olivocerebellar connections. Likewise, Schaumburg *et al.* reported that the dorsomedial nucleus and anterior nucleus of the thalamus were unremarkable in adrenoleukodystrophy cases lacking frontal lobe lesions.[20] Third, repeated episodes of epileptic convulsions may play a role in gray matter lesions, particularly in the hippocampus. The hippocampus is known to be vulnerable to epileptic convulsions, and hippocampal sclerosis is a characteristic neuropathological feature of epilepsy.[21] Among the cases presented here, the hippocampal gray matter lesions were most severe in Case 1, possibly corresponding to the history of more frequent convulsions than in the other two cases.

Among the remarkable clinical features seen in the present cases were the extrapyramidal symptoms in Case 1 (brachybasia and tremor) and Case 3 (brachybasia, rigidity and tremor), whereas a full neurological evaluation was not performed in Case 2 because of the multiple bone fractures. Although these symptoms can be considered to be a less prominent clinical manifestation than the other

symptoms, such as personality change, dementia and convulsions, only a few reports have described extrapyramidal symptoms in the clinical course of the disease.[3,22] Harada, for example, reported a case showing brachybasia, rigidity, masked face and tremor, and the case also exhibited atrophy in the basal ganglia. However, the origin of the symptoms of this disease remains unclear. In all the three cases presented here, neuronal loss was found in the basal ganglia as well as the substantia nigra, indicating that these may be responsible for the extrapyramidal symptoms. Nigro-striatal degeneration could be a constant pathological feature of Nasu-Hakola disease, at least in cases accompanied by extrapyramidal symptoms.

In conclusion, this study shows that the gray matter is commonly affected by neuronal loss and gliosis in Nasu-Hakola disease, with the exception of the cortical gray matter. These pathologies were prominent in the thalamus, caudate nucleus, putamen and substantia nigra, and the severity correlated with the disease duration in our series. These pathologies are considered to be responsible for some of the clinical manifestations of the disease, including the extrapyramidal symptoms.

ACKNOWLEDGMENTS

The authors thank Hiromi Kondo, Chie Haga and Yoko Shimomura for their expert technical support.

REFERENCES

1. Nasu T, Tsukahara Y, Terayama K, Mamiya N. An autopsy case of "membranous lipodystrophy" with myeloosteopathy of long bones and leucodystrophy of the brain. The 59th Tokyo Meeting of Pathology, Tokyo. *Tokyo Byori Shudankai Kiji* 1970; 10–13.
2. Hakola HPA, Järvi OH, Sourander P. Osteodysplasia polycystica hereditaria combined with sclerosing leucoencephalopathy, a new entity of the dementia praesenilis group. *Acta Neurol Scand Suppl* 1970; **43**: 78–79.
3. Hakola HPA. Neuropsychiatric and genetic aspects of a new hereditary disease characterized by progressive dementia and lipomembranous polycystic osteodysplasia. *Acta Psychiatr Scand Suppl* 1972; **232**: 1–173.
4. Pekkarinen P, Hovatta I, Hakola P *et al.* Assignment of the locus for PLO-SL, a frontal-lobe dementia with bone cysts, to 19q13. *Am J Hum Genet* 1998; **62**: 362–372.
5. Paloneva J, Kestilä M, Wu J *et al.* Loss-of-function mutations in TYROBP (DAP12) result in a presenile dementia with bone cysts. *Nat Genet* 2000; **25**: 357–361.
6. Paloneva J, Manninen T, Christman G *et al.* Mutations in two genes encoding different subunits of a receptor signaling complex result in an identical disease phenotype. *Am J Hum Genet* 2002; **71**: 656–662.
7. Bouchon A, Hernández-Munain C, Cella M, Colonna M. A DAP12-mediated pathway regulates expression of CC chemokine receptor 7 and maturation of human dendritic cells. *J Exp Med* 2001; **194**: 1111–1122.
8. Daws MR, Lanier LL, Seaman WE, Ryan JC. Cloning and characterization of a novel mouse myeloid DAP12-associated receptor family. *Eur J Immunol* 2001; **31**: 783–791.
9. Matsushita M, Oyanagi S, Hanawa S, Shiraki H, Kosaka K. Nasu-Hakola's disease (membranous lipodystrophy). A case report. *Acta Neuropathol* 1981; **54**: 89–93.
10. Sourander PA. New entity of phacomatosis:B.Brain lesions (Sclerosing leukoencephalopathy). *Acta Pathol Microbiol Scand Suppl* 1970; **215**: 44.
11. Amano N, Iwabuchi K, Sakai H *et al.* Nasu-Hakola's disease (membranous lipodystrophy). *Acta Neuropathol* 1987; **74**: 294–299.
12. Miyazu K, Kobayashi K, Fukutani Y *et al.* Membranous lipodystrophy (Nasu-Hakola disease) with thalamic degeneration: report of an autopsied case. *Acta Neuropathol* 1991; **82**: 414–419.
13. Kobayashi K, Kobayashi E, Miyazu K *et al.* Hypothalamic haemorrhage and thalamus degeneration in a case of Nasu-Hakola disease with hallucinatory symptoms and central hypothermia. *Neuropathol Appl Neurobiol* 2000; **26**: 98–101.
14. Paloneva J, Autti T, Raininko R *et al.* CNS manifestations of Nasu-Hakola disease: a frontal dementia with bone cysts. *Neurology* 2001; **56**: 1552–1558.
15. Mosley K, Cuzner ML. Receptor-mediated phagocytosis of myelin by macrophages and microglia: effect of opsonization and receptor blocking agents. *Neurochem Res* 1996; **21**: 481–487.
16. Smith ME. Phagocytosis of myelin by microglia in vitro. *J Neurosci Res* 1993; **35**: 480–487.
17. Tateishi J, Sato Y, Suetsugu M, Takashiba T. Adrenoleukodystrophy with olivopontocerebellar atrophy-like lesions. *Clin Neuropathol* 1986; **5**: 34–39.
18. Kakita A, Ishikawa A, Koike R, Tsuji S, Takahashi H. Adrenoleukodystrophy with involvement of the cerebral cortex. *Neuropathology* 1997; **17**: 106–111.
19. Sima AA, Pierson CR, Woltjer RL *et al.* Neuronal loss in Pelizaeus-Merzbacher disease differs in various mutations of the proteolipid protein 1. *Acta Neuropathol* 2009; **118**: 531–539.
20. Schaumburg HH, Powers JM, Raine CS, Suzuki K, Richardson EP Jr. Adrenoleukodystrophy. A clinical

and pathological study of 17 cases. *Arch Neurol* 1975; **32**: 577–591.
21. Fujikawa DG, Itabashi HH, Wu A, Shinmei SS. Status epilepticus-induced neuronal loss in humans without systemic complications or epilepsy. *Epilepsia* 2000; **41**: 981–991.
22. Harada K. A case of "membranous lipodystrophy (Nasu)" with emphasis on psychiatric and neuropathologic aspects (author's transl). *Folia Psychiatr Neurol Jpn* 1975; **29**: 169–177.

Neuroscience 177 (2011) 298–307

EFFECT OF GLYCOGEN SYNTHASE KINASE 3 β-MEDIATED PRESENILIN 1 PHOSPHORYLATION ON AMYLOID β PRODUCTION IS NEGATIVELY REGULATED BY INSULIN RECEPTOR CLEAVAGE

M. MAESAKO,[a] K. UEMURA,[b] M. KUBOTA,[a] K. HIYOSHI,[a] K. ANDO,[b] A. KUZUYA,[b] T. KIHARA,[c] M. ASADA,[a] H. AKIYAMA[d] AND A. KINOSHITA[a]*

[a]*School of Human Health Sciences, Kyoto University Graduate School of Medicine, Kyoto 606-8507, Japan*

[b]*Department of Neurology, Kyoto University Graduate School of Medicine, Kyoto 606-8507, Japan*

[c]*Department of Neuroscience for Drug Discovery, Kyoto University Graduate School of Pharmaceutical Sciences, Kyoto 606-8501, Japan*

[d]*Tokyo Institute of Psychiatry, Tokyo 156-8585, Japan*

Abstract—Presenilin 1 (PS1), a causative molecule of familial Alzheimer's disease (AD), is known to be an unprimed substrate of glycogen synthase kinase 3 β (GSK3β) [Twomey and McCarthy (2006) FEBS Lett 580:4015–4020] and is phosphorylated at serine 353, 357 residues in its cytoplasmic loop region [Kirschenbaum et al. (2001) J Biol Chem 276:7366–7375]. In this report, we investigated the effect of PS1 phosphorylation on AD pathophysiology and obtained two important results—PS1 phosphorylation increased amyloid β (Aβ) 42/40 ratio, and PS1 phosphorylation was enhanced in the human AD brains. Interestingly, we demonstrated that PS1 phosphorylation promoted insulin receptor (IR) cleavage and the IR intracellular domain (IR ICD) generated by γ-secretase led to a marked transactivation of Akt (PKB), which downregulated GSK3β activity. Thus, the cleavage of IR by γ-secretase can inhibit PS1 phosphorylation in the long run. Taken together, our findings indicate that PS1 phosphorylation at serine 353, 357 residues can play a pivotal role in the pathology of AD and that the dysregulation of this mechanism may be causally associated with its pathology.

Key words: Alzheimer's disease, presenilin 1, phosphorylation, regulated intramembrane proteolysis, insulin receptor, Akt.

Alzheimer's disease (AD) is pathologically characterized by amyloid plaques and neurofibrillary tangles (NFTs). Amyloid plaques are composed of amyloid β (Aβ) peptides, which are derived from amyloid precursor protein (APP) via proteolytic cleavage by γ-secretase (De Strooper et al., 1998). γ-Secretase is an enzymatic complex composed of at least four proteins: Presenilin 1 or Presenilin 2 (PS1 or PS2), Nicastrin, Pen 2, and Aph 1, with Presenilin representing the catalytic core (Yu et al., 2000; Francis et al., 2002; Goutte et al., 2002). PS1 mutations account for the majority of cases of familial AD, and more than 170 pathogenic mutations have been identified within the PS1 coding sequence. On the other hand, NFTs are characterized by the accumulation of hyperphosphorylated Tau in neurons (Grundke-Iqbal et al., 1986). One of the candidates which phosphorylate Tau is glycogen synthase kinase 3 β (GSK3β) (Hanger et al., 1992).

GSK3β, originally known to inactivate glycogen synthesis, is a serine/threonine protein kinase with a wide variety of substrates, and is expressed in various tissues with the highest level in the brain (Grundke-Iqbal et al., 1986). Interestingly, GSK3β phosphorylates not only Tau but also PS1 at serine 353, 357 residues in its cytoplasmic loop region (Kirschenbaum et al., 2001; Twomey and McCarthy, 2006). Therefore, it is intriguing to examine the function of PS1 phosphorylation at those residues to connect two AD hallmarks—amyloid plaques and NFTs. Although our recent report demonstrated that GSK3β-mediated PS1 phosphorylation regulates the localization of γ-secretase and inhibits its N-cadherin cleavage (Uemura et al., 2007), a direct impact of PS1 phosphorylation on AD pathogenesis has not been elucidated so far.

Here, we demonstrate that GSK3β-mediated PS1 phosphorylation inhibits APP cleavage by γ-secretase activity and decreases the total Aβ production whereas it increases Aβ 42/40 ratio. Importantly, we found that PS1 phosphorylation was enhanced in the human AD brains. To further elucidate the underlying mechanisms which regulate PS1 phosphorylation, we focused on insulin signaling. We observed that phosphorylated PS1 promotes the cleavage of insulin receptor (IR) by γ-secretase activity. Intracellular domain of IR (IR ICD), produced by the cleavage, enhances the transcription of Akt (PKB), leading to inhibit GSK3β activity. Therefore, we propose that PS1, localized downstream of GSK3β, may play a pivotal role in Aβ production under the influence of insulin signaling, a mechanism that may be deeply associated with AD pathophysiology.

EXPERIMENTAL PROCEDURES

Human brain samples

From the brain tissue collection in Tokyo Institute of Psychiatry (H.A.), which mainly consists of cases from psychogeriatric wards, we employed experiments of six dementia patients' brains with CERAD plaque score "C" (Mirra et al., 1991) and Braak and

*Corresponding author. Tel: +81-75-751-3969; fax: +81-75-751-3969.
E-mail address: akinoshita@hs.med.kyoto-u.ac.jp (A. Kinoshita).

Abbreviations: AD, Alzheimer's disease; APP, amyloid precursor protein; Aβ, amyloid β; CTF, C-terminal fragment; FBS, fetal bovine serum; GSK3β, glycogen synthase kinase 3 β; ICD, intracellular domain; IR, insulin receptor; MEF, mouse embryonic fibroblast; NFTs, neurofibrillary tangles; NTF, N-terminal fragment; PS1, presenilin 1; RIP, regulated intramembrane proteolysis.

0306-4522/11 $ - see front matter
doi:10.1016/j.neuroscience.2010.12.017

Table 1. Characteristics of human brain samples

	Case	Age (y)	Sex	Postmortem interval (h)	Clinical diagnosis	Pathological findings
1	Schizophrenia	75	M	15	Schizophrenia	Plaque(−), NFT stage II, minor stroke
2	Aortic rupture	80	F	2	Aortic rupture	Plaque(−), tangle(−)
3	Cirrhosis of the liver	77	M	7.5	Cirrhosis of the liver	Plaque(−), NFT stage I
4	Alcoholism	60	M	5	Alcoholism	Plaque(−), tangle(−)
5	Fahr disease	48	M	10	Fahr disease	Plaque(−), tangle(−)
6	AD①	75	M	12	Alzheimer's disease	Braak stage C, VI
7	AD②	68	F	9	Alzheimer's disease	Braak stage C, VI
8	AD③	75	M	17.5	Alzheimer's disease	Braak stage C, VI
9	AD④	77	M	2	Alzheimer's disease	Braak stage C, VI
10	AD⑤	87	F	6	Alzheimer's disease	Braak stage C, VI
11	AD⑥	56	M	18	Alzheimer's disease	Braak stage C, VI

We employed experiments of six Alzheimer's disease patients' brains, as well as five control subjects without neurological complications. Fresh-frozen samples were taken in all cases from the mediobasal temporal neocortex. There is no statistical difference in the postmortem interval between AD and control cases.

Braak's NFTs stage IV or higher (Braak and Braak, 1991), as those with AD, as well as five control subjects without neurological complications (Table 1). Fresh-frozen samples were taken in all cases from the mediobasal temporal neocortex. The brain samples were extracted in RIPA buffer (50 mM Tris–HCl, 150 mM NaCl, 1% Triton X100, 1% NP-40, 0.5% Deoxycholate, 0.1% SDS, pH 8.0) with protease inhibitor cocktail (Roche, Switzerland) and sufficiently homogenized on ice. Then the samples were incubated for one night at 4 °C and centrifuged at 14,000 g×20 min. The supernatants were directly used for Western blot analysis. All autopsies were undertaken with written consents and the study was approved by the official ethical committees of Kyoto University as well as of Tokyo Institute of Psychiatry.

Plasmid constructs

The pcDNA3.1-hIR (human Insulin Receptor) construct was a kind gift from Dr. Ikeuchi (Niigata University, Japan) (Ebina et al., 1985). The cDNA encoding the IR ICD was generated by polymerase chain reaction (PCR) using the following primers: IR ICD forward, CGGGTACCCGCCATGAGAAAGAGGCAGCCAGA, and IR ICD reverse, CGGGATCCGGAAGGATTGGACCGAGGCAA. The PCR product was subcloned into the reading frame of the Kpn1/BamH1 sites of the pcDNA3 with HA tag vector. The construction of the plasmids expressing wt PS1, pseudo-phosphorylation PS1 (S353/357D PS1), deletion mutant PS1 (Δ340-350 PS1), and dominant negative PS1 (D385A PS1) was described previously (Uemura et al., 2003, 2007). Precise cloning of all reading frames was verified by sequencing.

Cell culture and transfection

SH-SY5Y (derived from human neuroblastoma) cells were maintained in Opti-MEM containing 10% fetal bovine serum (FBS) (Invitrogen, USA). Establishment of cell lines which stably express hIR was described previously (Maesako et al., 2010). PS1/PS2 double knockout mouse embryonic fibroblast (MEF PS-/-) cells were generously donated by Dr. B De Strooper and they were maintained in Dulbecco's modified Eagle's medium (DMEM) (SIGMA, USA) with 10% FBS. CHO cells stably expressing both Swedish mutant APP (K670M/N770L) and human N-cadherin (APPsw/Ncad-CHO cells) were obtained and maintained as described previously (Uemura et al., 2007). For transient transfection into SH-SY5Y as well as into MEF PS-/- cells, cells were plated in 6-cm dishes with serum-containing medium. 8 μg of plasmid DNA and 20 μl of TransFectin reagent (Bio-Rad, USA) were mixed into 1 ml of serum-free medium and incubated for 20 min, then added directly to confluent cells in 2 ml of serum-containing medium. 24 to 48 h after transfection, reporter gene activity was assayed.

Antibodies and chemical reagents

Anti-IR, a monoclonal antibody recognizing the C-terminal amino acid residues of human IR, was from Neo Markers. Rabbit polyclonal anti-Akt and phospho-GSK3β (S9) were from Cell Signaling Technology. Mouse monoclonal anti-GSK3β was from BD Transduction Laboratories. Mouse monoclonal anti-β-actin and rabbit polyclonal anti-APP C-terminal antibodies were from SIGMA. Rabbit polyclonal anti-PS1 NTF and goat polyclonal phospho-PS1 (S353/357) antibodies were from Santa Cruz. Mouse monoclonal PS1 CTF antibody was from Calbiochem. Alexa Fluor 546 anti-mouse IgG and Alexa Fluor 488 anti-goat IgG were obtained from Molecular Probes. γ-secretase inhibitor DAPT and L-685458 were from SIGMA. Akt inhibitor IV, TPA, and PKC inhibitor were from Calbiochem. Insulin solution was from SIGMA and DMSO was from Nacalai tesque.

Western blotting

Cells were washed in phosphate-buffered saline (PBS) two times and scraped off. Cell pellets were suspended in ice-cold TNE buffer (10 mM Tris–HCl, 150 mM NaCl, 1% NP-40, 1 mM EDTA pH 7.8), supplemented with protease inhibitor cocktail, and briefly subjected to sonication. The samples were centrifuged at 14,000 g×20 min at 4 °C and the supernatants were collected to obtain protein samples. The protein concentration was determined using the Bradford assay (Bradford, 1976). Protein samples were diluted with sample buffer (125 mM Tris, 4% SDS, 2% 2-mercaptoethanol, 20% glycerol and 0.01% Bromophenol Blue, pH 6.8) and denatured at 95 °C for 5 min. Samples containing equal amounts of protein were electrophoresed on polyacrylamide gradient gels (5–20%) (Atto, Japan) in running buffer (25 mM Tris, 192 mM glycine, 0.1% SDS). In this gel, APP C-terminal fragments (CTFs) bands were shown as a single band. To detect APP ICD (AICD), samples were electrophoresed on 15% Tricine gels (Atto, Japan) in Tricine SDS Running Buffer. Immunoblotting was carried out by transferring the proteins to polyvinylidene difluoride microporous membrane, blocking this membrane with 5% skimmed milk in 20 mM TBS containing 0.1% Tween 20 (TBS-T), and incubating with the primary antibodies in PBS containing 4% bovine serum albumin (BSA) (Nacalai tesque, Japan) overnight at 4 °C. The membranes were then washed in TBS-T and incubated with a horseradish peroxidase-conjugated anti-mouse IgG (GE Healthcare, UK) in TBS-T for 1 h at room temperature. The specific reaction

was visualized using the enhanced chemiluminescence (ECL) method (GE Healthcare).

In vitro γ-secretase assay

To analyze AICD or IR ICD level by *in vitro* γ-secretase assay (Sastre et al., 2001), cells were suspended (0.5 ml/10 cm dish) in homogenization buffer (10 mM MOPS, 10 mM KCl, pH 7.0) and homogenates and the post-nuclear supernatant (PNS) were prepared as described (Steiner et al., 1998). Membranes were pelleted from the PNS by centrifugation for 20 min at 16,000 g at 4 °C, washed with homogenization buffer and resuspended (50 μl/10 cm dish) in assay buffer (150 mM sodium citrate, pH 6.4). To allow generation of ICD, samples were incubated at 37 °C for 2 h in a volume of 25 μl/ assay. Control samples were kept at 4 °C. After termination of the assay reactions, samples were separated into pellet fractions (membrane fractions) and supernatant fractions by ultracentrifugation for 1 h at 100,000 g at 4 °C. AICD was detected using polyclonal anti-APP C-terminal antibody and IR ICD was detected using monoclonal anti-IR C-terminal antibody.

Immunostaining

5.0×10^4 cells were harvested onto 0.1% polyethyleneimine-coated Lab-Tek II Chamber slides (four-well; Nalge Nunc International, Rochester) and maintained in Opti-MEM containing 10% FBS. Cells were cultured for the indicated time and then fixed with 4% paraformaldehyde for 20 min. Fixed cells were blocked with PBS containing 0.2% Triton X-100 for 15 min and incubated overnight at 4 °C with each antibody diluted in PBS containing 3% BSA. Immunoreactivity was visualized using the species-specific secondary antibodies mentioned above. The samples were examined using a laser confocal scanning microscope, LSM 510 Pascal (Zeiss, Switzerland).

Measurement of extracellular Aβ

The levels of Aβ 40 and Aβ 42 were measured by ELISA kits specific to Aβ 40 and Aβ 42 (Wako, Japan), as described previously (Uemura et al., 2009). Briefly, APPsw/Ncad-CHO cells were cultured in 6 cm dishes at a density of 7.0×10^5 cells /well. 24 h after incubation, the cells were treated with reagents for 5 h in DMEM/F-12 medium, followed by replacing DMEM/F-12 with 6 ml of Opti-MEM. 1 h after replacing, 1 ml of medium was collected, centrifuged at 600 g for 5 min, and 100 μl of the aliquot was used for measurement of extracellular Aβ.

MTT assay

The viability in APPswe/N-cad-CHO cells was analyzed by MTT assay using MTT Cell Proliferation Assay Kit (Cayman Chemical Co., USA). Briefly, cells were cultured in a 96-well plate at a density of 1.0×10^4 cells/well. 24 h after incubation, reagents of indicated concentration were treated for 5 h in the presence of DMEM/F-12 medium, followed by replacing DMEM/F-12 with 100 μl of Opti-MEM with the reagents. 1 h after replacing, MTT was measured using the Kit and microplate reader.

Real-time PCR assay

Total RNA was isolated using ISOGEN (NIPPON GENE, Japan), according to the manufacture's protocol. For real-time PCR analysis, 5 μg total RNA from each sample was used for cDNA synthesis kit (GE Healthcare). Real-time PCR primers were designed as follows: Akt1: fw GACCTCAAGCTGGAGAAC/rv ACTGCACGGCCGTAGTC, Akt2: fw ACCGCCTGTGCTTTGTGATG/rv TCATTGTCCTCCAGCACCTC, Akt3: fw CATTATTGCAAAGGATGAAGTGGCAC/rv CCAGCATTAGATTCTCCAACTTGAG.

For the amplification of Akt, 5 μl of cDNA was added to the SYBR green master mix (Roche) and real-time PCR assay was performed in LightCycler 480 (Roche).

Statistical analysis

All values are given in means±SE. Comparisons were performed using an unpaired Student's *t*-test. For comparison of multiparametric analysis, one-way factorial ANOVA, followed by the post hoc analysis by Fisher's PLSD was used. $P<0.05$ was considered to indicate a significant difference. $n=4$ indicated four independent experiments.

RESULTS

PS1 phosphorylation inhibits APP cleavage but enhances extracellular Aβ 42/40 ratio

Since PS1 is known to be the essential component of γ-secretase, we examined the effect of its phosphorylation on APP cleavage. To test this, we transfected wt PS1 and pseudo-phosphorylated PS1 mutant S353/357D PS1 (in which serine residues phosphorylated by GSK3β are substituted with aspartate to mimic phosphorylation state; Uemura et al., 2007) into MEF PS-/- cells. Transfected cells were treated with insulin to promote ectodomain shedding (Linda et al., 2007) and to inhibit the phosphorylation of wt PS1 (Maesako et al., 2010). APP CTFs band was accumulated in MEF PS-/- cells (Fig. 1A, first lane). Interestingly, in the absence of insulin, the level of APP CTFs was slightly higher in S353/357D PS1 cells than that in wt PS1 (Fig. 1A, second and third lanes). Moreover, in the presence of insulin, the level of APP CTFs in S353/357D PS1 was significantly increased compared to that in wt PS1 (Fig. 1A, fourth and fifth lanes, Fig. 1B). Using Tricine gels, we could detect that the level of AICD in S353/357D PS1 was decreased compared to that in wt PS1 (Fig. 1C, third and fourth lanes). This result was confirmed by *in vitro* γ-secretase assay (Fig. 1D). Collectively, these results suggested that PS1 phosphorylation inhibited the γ-secretase-mediated cleavage of APP CTFs.

As Aβ plays a pivotal role in the pathogenesis of AD, we next examined the effect of PS1 phosphorylation on extracellular Aβ production, as well as Aβ 42/40 ratio. For this purpose, either Akt inhibitor IV or LiCl, which activates or inhibits GSK3β respectively, was added to change the phosphorylation status of PS1 in APPswe/N-cad-CHO cells (Fig. 1E). Under this condition, neither of them induced cell death (Fig. 1F). Interestingly, Akt inhibitor significantly decreased the amount of extracellular Aβ 40 whereas LiCl significantly increased its amount (Fig. 1G). In contrast, the extracellular Aβ 42 level in the presence of either Akt inhibitor or LiCl remained almost the same (Fig. 1H), thus leading to the increase of Aβ 42/40 ratio in Akt inhibitor-treated cells or to the decrease of its ratio in LiCl-treated cells (Fig. 1I). These results collectively indicate that GSK3β-mediated PS1 phosphorylation down-regulated Aβ production but enhanced Aβ 42/40 ratio.

PS1 phosphorylation is enhanced in AD human brain samples

It was reported that GSK3β activity was up-regulated in AD brains (Bhat et al., 2004). Therefore, we assumed that the phosphorylation ratio of PS1 might be increased in AD brains. Thus, we analyzed the phosphorylation ratio of PS1

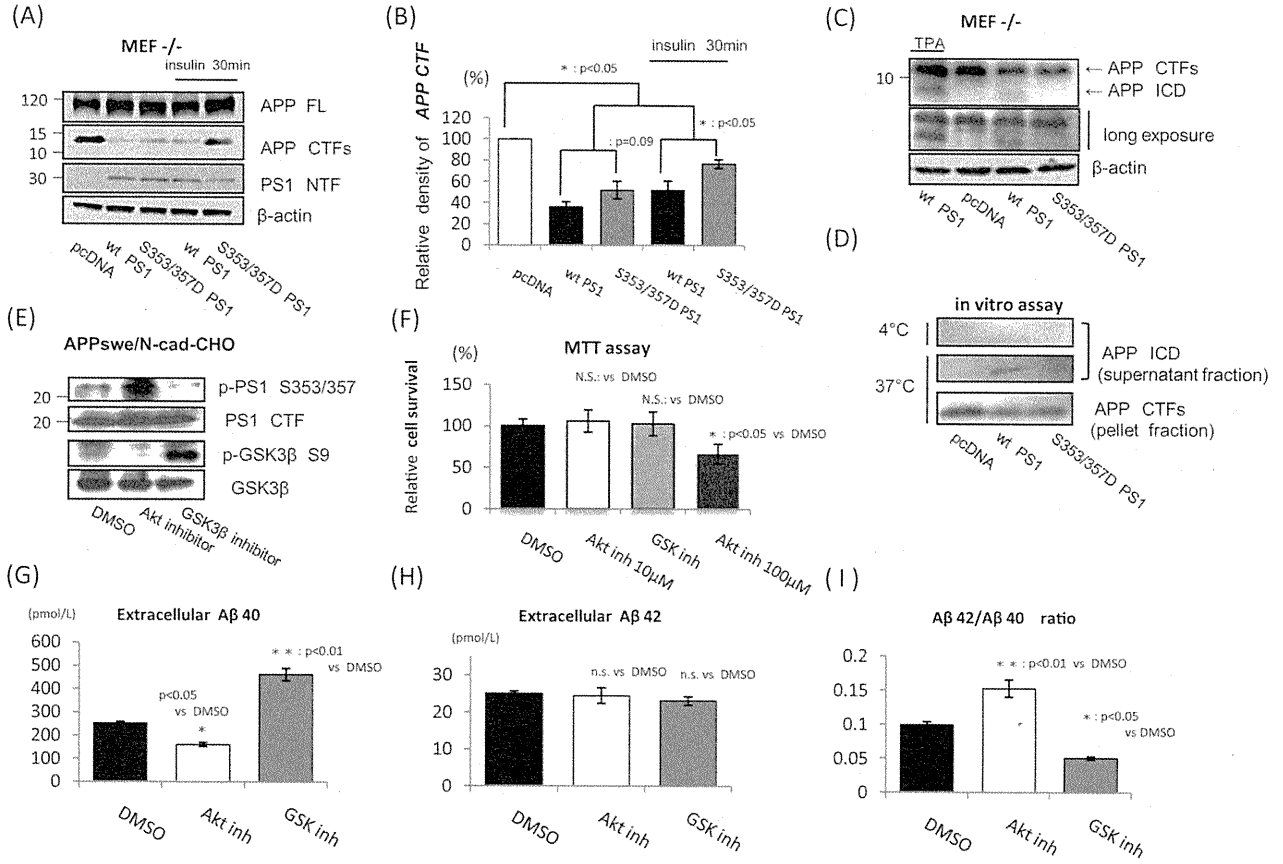

Fig. 1. PS1 phosphorylation inhibits APP cleavage but enhances extracellular Aβ 42/40 ratio. (A) Either wt PS1 or pseudo-phosphorylation PS1 mutant (S353/357D PS1) was transfected into MEF PS-/- cells. Control cells were transfected with pcDNA (first lane). 24 h after transfection, cells were treated with 50 nM insulin for 30 min (fourth and fifth lanes). (B) APP CTFs were normalized by housekeeping gene (β-actin) and relative band density was quantitatively analyzed (n=3). (C) Either wt PS1 or S353/357D PS1 was transfected into MEF PS-/- cells and APP ICD was detected by Tricin-SDS-PAGE using anti APP-C-terminal antibody. Cells were treated with 500 nM TPA that promoted the processing of APP as a positive control. (D) Membrane preparations from MEF PS-/- cells transfected with pcDNA, wt PS1 or S353/357D PS1 were incubated at 37 °C for 2 h. Control samples were kept at 4 °C. The reaction mix was then separated in pellet fraction as membrane fraction (lower panel) and supernatant fraction (first and second panels) by ultracentrifugation. These fractions were electrophoresed on polyacrylamide gradient gels or Tricine gels and immunoblotted with anti APP-C-terminal antibody. (E) APPsw/Ncad-CHO cells were incubated in Opti-MEM in the presence of 10 μM Akt inhibitor IV or 25 mM LiCl for 6 h. PS1 (S353/357) and GSK3β (S9) phosphorylation were analyzed by immunoblotting, using anti-phospho-PS1 S353/357, anti-PS1 CTF, anti-GSK3β and anti-phospho-GSK3β S9 antibodies. (F) Cell viability was analyzed by MTT assay. Both 10 μM of Akt inhibitor IV and 25 mM LiCl (GSK inhibitor) which were used in this study didn't induce cell death (n=10). 100 μM of Akt inhibitor was used as positive control. (G) and (H) APPsw/Ncad-CHO cells were incubated in Opti-MEM in the presence of 10 μM Akt inhibitor IV or 25 mM LiCl for 6 h. DMSO was used as a negative control. After incubation, released extracellular Aβ 40 or Aβ 42 for 1 h were analyzed by ELISA (n=5). (I) Extracellular Aβ 42/40 ratio was quantitatively analyzed.

in human brains. In order to rule out the post-mortem effect on the phosphorylation state of PS1 and GSK3β, we examined the levels of PS1 and GSK3β phosphorylation in mouse brains with different post-mortem intervals and demonstrated that post-mortem intervals did not influence the phosphorylation ratio of either PS1 or GSK3β up to 36 h after sacrifice (data not shown). In accordance with the previous reports, the phosphorylation ratio of GSK3β S9 was significantly decreased in AD brains compared with that in control brains (Fig. 2A, third and fourth rows, Fig. 2B), indicating the hyperactivity of GSK3β in AD brains. In contrast, PS1 phosphorylation was significantly increased in AD brains compared with that in control ones (Fig. 2A, first and second rows, Fig. 2C). These results suggest that up-regulated GSK3β activity could enhance PS1 phosphorylation in AD-affected brains.

PS1 phosphorylation promoted IR cleavage

Since IR is one of key regulators of GSK3β activity, we analyzed the functional relationship between PS1/γ-secretase activity and IR. It is now reported that γ-secretase processes IR, a main player of insulin signaling, along with other substrates (Kasuga et al., 2007; Marambaud et al., 2002; Okamoto et al., 2001). As reported previously, ectodomain shedding of IR β-subunit by metalloproteases generates a membranous fragment—IR CTF (Fig. 3A, bottom), which is further cleaved by γ-secretase to produce the intracellular domain—IR ICD (Fig. 4A, bottom). For the analysis of IR cleavage, we co-transfected either wt PS1 or S353/357D PS1 together with IR into MEF PS-/- cells, followed by insulin treatment. In the absence of insulin, IR CTF level was slightly higher in wt PS1 cells than that in

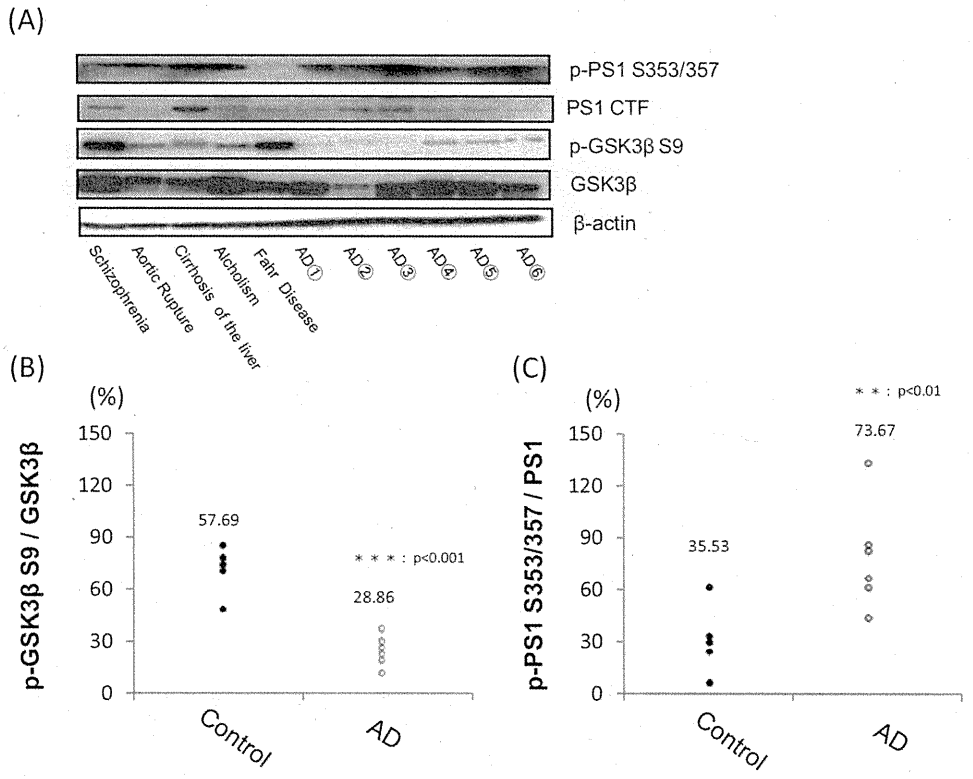

Fig. 2. PS1 phosphorylation is increased in AD brains. (A) The lysates of human brain samples, including AD and non-AD brains, were analyzed by immunoblotting, using anti-phospho-PS1 S353/357, anti-PS1 CTF, anti-GSK3β and anti-phospho-GSK3β S9 antibodies. Lording control was detected using anti-β-actin antibody (lower panel). (B, C) GSK3β and PS1 phosphorylation ratio of each sample was quantitatively analyzed and described as a point. The number indicated on the point means average ratio.

S353/357D PS1 cells (Fig. 3B, second and third lanes). Moreover, insulin treatment led to a robust increase in the level of IR CTF in wt PS1 when compared to that in S353/357D PS1 (Fig. 3B, fourth and fifth lanes, Fig. 3C). In addition, we examined the level of IR ICD using *in vitro* γ-secretase assay and demonstrated that IR ICD level in S353/357D PS1 cells was higher than that in wt PS1 cells (Fig. 3D). These results suggested that PS1 phosphorylation enhanced the γ-secretase-mediated cleavage of IR CTF.

Since phosphorylation of PS1 reduces the PS1/N-cadherin/β-catenin interaction (Uemura et al., 2007), we asked whether the PS1 interaction with N-cadherin/β-catenin directly affects IR cleavage. To test this, MEF PS-/- cells were co-transfected with IR and Δ340-350 PS1 (a deletion mutant lacking the loop domain necessary for the interaction with N-cadherin/β-catenin; Uemura et al., 2007), followed by insulin treatment. As in S353/357D PS1 transfected cells (Fig. 3E, middle lane), the level of IR CTF in Δ340-350 PS1 transfected cells was significantly decreased compared to that in wt PS1 cells (Fig. 3E, left and right lanes, Fig. 3F). These findings were also confirmed in neuronal cells (Fig. 3G). Collectively, these results indicated that dissociation of PS1 from N-cadherin/β-catenin as well as phosphorylation of PS1 promotes the cleavage of IR by γ-secretase.

IR intracellular domain up-regulates the transcription of Akt

Several lines of evidence suggest that the cleavage of membrane protein by γ-secretase, known as regulated intramembrane proteolysis (RIP), is linked to intracellular signaling events (Wolfe and Kopan, 2004; Maetzel et al., 2009). γ-secretase generates the intracellular domain (ICD) of the membranous proteins, resulting in the release of ICD from the membrane. Some ICDs translocate to the nucleus and act as transcription regulators. IR ICD also translocates to the nucleus (Kasuga et al., 2007), but its exact function remains unknown.

To examine the cellular consequence of IR-RIP, we transfected IR ICD fused with HA-Tag (Fig. 4A, bottom) into SH-SY5Y cells. Immunostaining with anti-HA antibody revealed that IR ICD was located at the nucleus as in the previous report (Fig. 4B, under panel), whereas full length IR was located at the cell membrane and in the cytoplasmic region (Fig. 4B, top panel). In order to analyze the effect of IR ICD translocation into the nucleus we transiently transfected IR ICD into native SH-SY5Y cells. 36 h after transfection, mRNA was extracted and analyzed by real-time PCR assay. In this experiment, we focused on the mRNA level of Akt, because Akt plays important roles in IR signaling. Since Akt has three isoforms—Akt 1, 2 and 3, we evaluated mRNA level of all the isoforms. mRNA

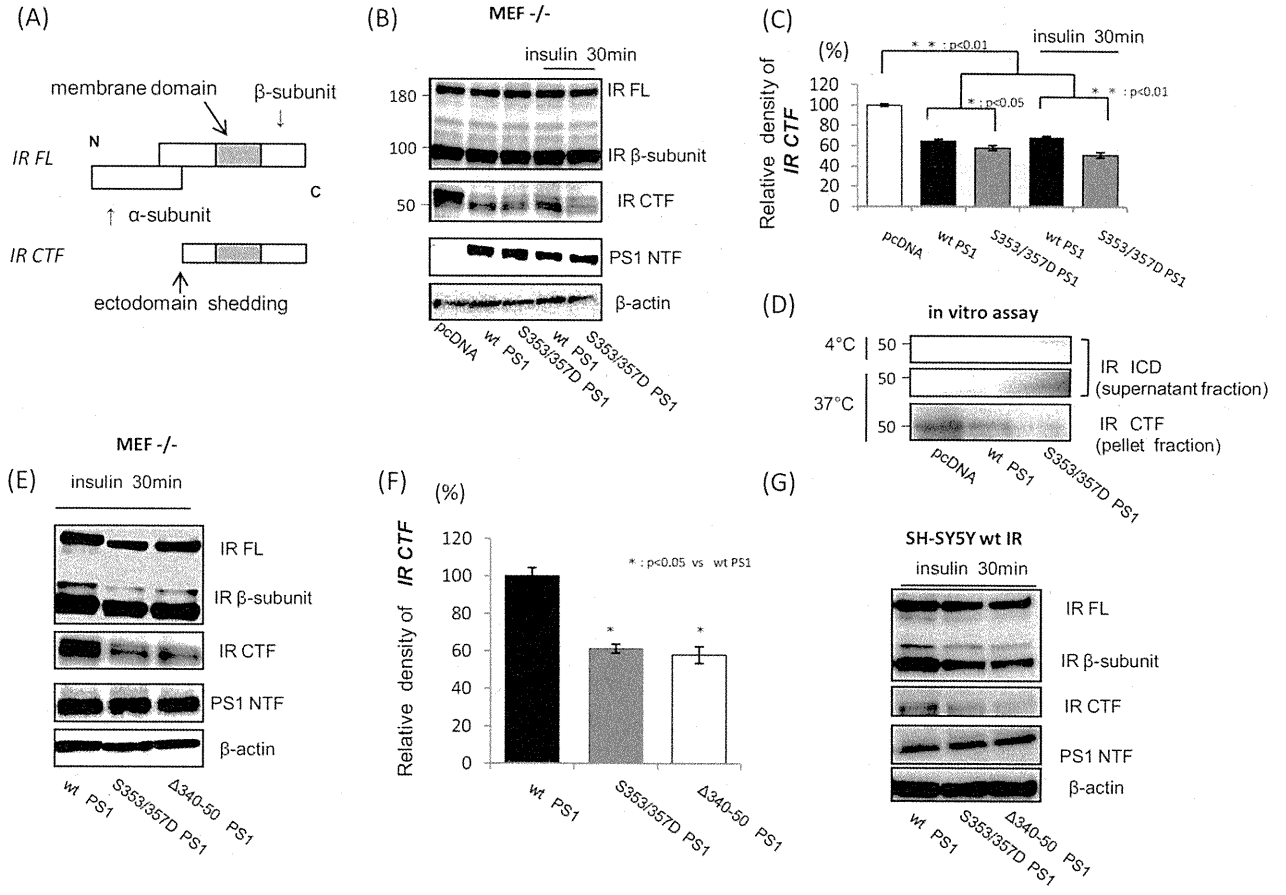

Fig. 3. IR cleavage is promoted by PS1 phosphorylation. (A) A schematic representation of IR CTF. IR-β-subunit is cleaved by metalloproteases at the extracellular area, producing IR CTF (bottom). (B) Either wt PS1 or S353/357D PS1 was co-transfected with IR into MEF PS-/- cells. Control cells were transfected with pcDNA (first lane). 24 h after transfection, cells were treated with 50 nM insulin for 30 min (fourth and fifth lanes). (C) IR CTF was normalized by β-actin and relative band density was quantitatively analyzed (n=3). (D) Membrane preparations from MEF PS-/- cells co-transfected IR with pcDNA, wt PS1 or S353/357D PS1 were incubated at 37 °C for 2 h. Control samples were kept at 4 °C. The reaction mix was then separated in pellet fraction as membrane fraction (lower panel) and supernatant fraction (first and second panels) by ultracentrifugation. These fractions were electrophoresed on polyacrylamide gradient gels and immunoblotted with anti IR-C-terminal antibody. (E) MEF PS-/- cells were transfected with wt PS1, S353/357D PS1 or Δ340-350 PS1 and after 24 h of transfection, cells were treated with 50 nM insulin for 30 min. (F) IR CTF was normalized by β-actin and relative band density was quantitatively analyzed (n=3). (G) SH-SY5Y wt IR cells were transfected with either wt PS1, S353/357D PS1 or Δ340-350 PS1 and then treated with 50 nM insulin for 30 min.

levels of Akt 1 and 2 were significantly increased in IR ICD transfected cells, compared with those in control cells (Fig. 4C). The protein level of total Akt was also significantly increased in IR ICD transfected cells 48 h after transfection (Fig. 4D, E), suggesting marked transactivation of Akt in IR ICD transfected cells. Moreover, under the same condition, we observed that IR ICD reduced GSK3β activity, promoted GSK3β S9 phosphorylation, as well as enhanced Akt levels (Fig. 4F, G). These results collectively indicate that IR ICD can enhance Akt transcription, followed by the reduction in GSK3β activity.

PS1/γ-secretase-mediated IR cleavage changes the expression level of Akt

To confirm that IR-RIP regulates the transcription of Akt, we modulated IR cleavage in several ways. First, we inhibited γ-secretase activity and observed the expression level of Akt. After a 24 h DAPT treatment, the level of Akt did not change in SH-SY5Y cells which have little endogenous IR (data not shown). On the other hand, the expression level of Akt was dose-dependently decreased in SH-SY5Y wt IR cells (Fig. 5A, top row), indicating that inhibition of γ-secretase led to decrease the levels of Akt. These results were confirmed by the treatment with another γ-secretase inhibitor, L-685458 (data not shown), and by non-pharmacological inhibition (Fig. 5B, middle and right lanes), using D385A PS1, which dominant-negatively inhibits γ-secretase activity (Uemura et al., 2003).

It was reported that IR might undergo ectodomain shedding by metalloproteases such as ADAM 17 (Kasuga et al., 2007). Since protein kinase C activation enhances the metalloprotease-mediated ectodomain shedding (Ni et al., 2001), we treated SH-SY5Y wt IR cells with 500 nM TPA to enhance the ectodomain shedding. In the presence of L-685458, TPA treatment for 24 h increased the level of IR CTF, indicating that ectodomain shedding of IR was

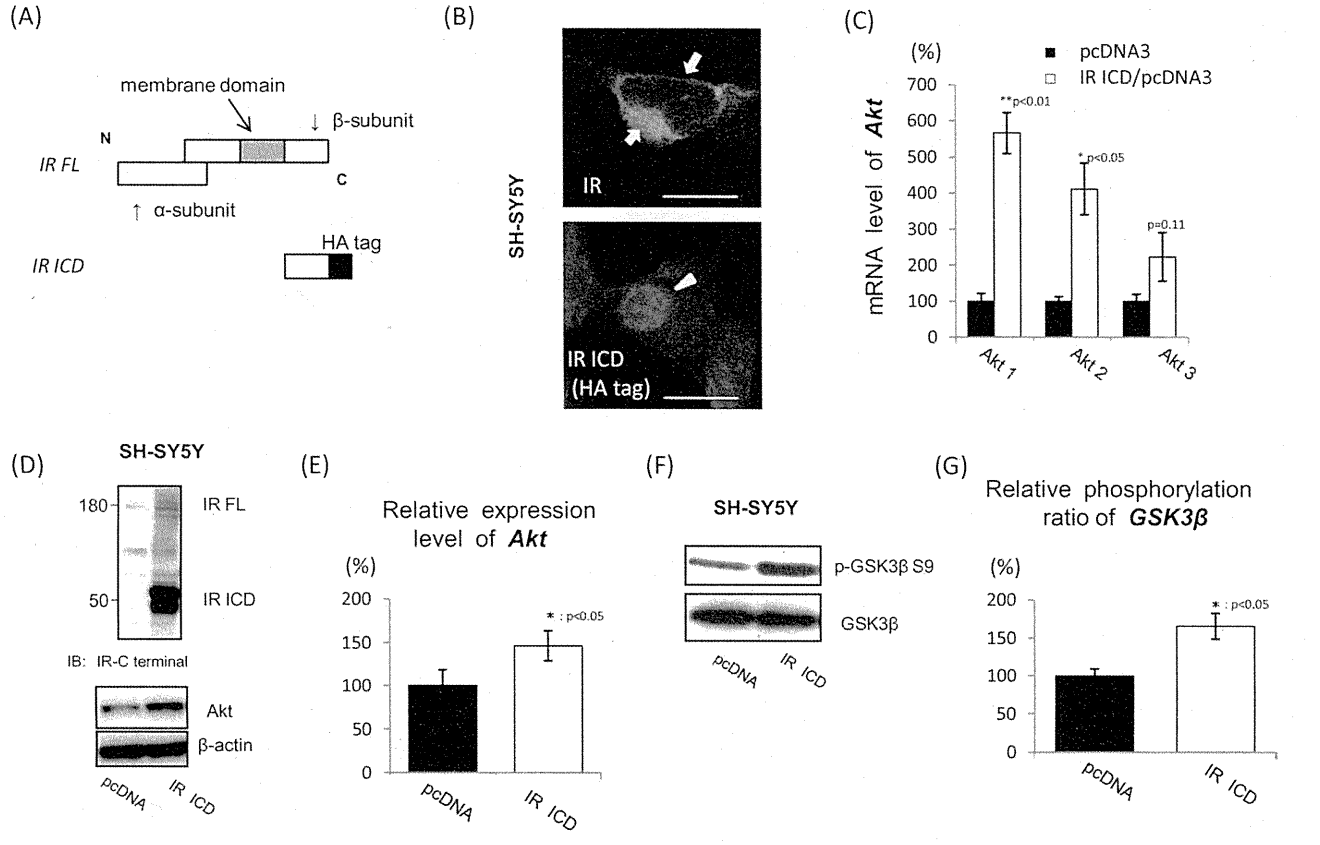

Fig. 4. IR ICD up-regulates the transcription of Akt. (A) A schematic representation of plasmid construction of IR ICD. The HA tag was fused to the C-terminus of IR ICD (bottom). The amino acid of transmembrane domain was indicated (top, gray area). (B) Native SH-SY5Y cells were transfected with IR ICD or full length (FL) IR. Scale bar, 20 μm. (C) SH-SY5Y cells were transfected with IR ICD. After 36 h of transfection, the mRNA levels of Akt were analyzed by real-time PCR assay. The mRNA amount of Akt was normalized by that of β-actin (n=4). (D) After 48 h of transfection, SH-SY5Y cells were analyzed by immunoblotting. (E) The expression level of endogenous Akt was quantitatively analyzed (n=3). The level of Akt was normalized by that of β-actin. (F) After 48 h of transfection of IR ICD, the level of phospho-GSK3β S9 was analyzed by immunoblotting. (G) The relative phosphorylation ratio of GSK3β was quantitatively analyzed (n=3).

promoted by TPA (Fig. 5C, third and fifth lanes). To analyze its effect on Akt levels, SH-SY5Y wt IR cells were pre-incubated with either DAPT or vehicle (DMSO) for 18 h, followed by TPA treatment with or without DAPT. Interestingly, in the absence of DAPT, the expression level of Akt was increased (Fig. 5D, fifth lane, Fig. 5E). Conversely, TPA treatment in the presence of DAPT significantly decreased the level of Akt (Fig. 5D, fourth and sixth lanes). Similarly, treatment with PKC inhibitor for 24 h in different concentrations demonstrated the dose-dependent decrease of Akt levels (data not shown). Taken together, these results indicate that γ-secretase-mediated IR cleavage generates IR ICD, which then transactivates Akt.

DISCUSSION

Previous reports demonstrated that GSK3β activity is up-regulated in AD brains (Bhat et al., 2004). On the other hand, conditional transgenic mice overexpressing GSK3β in the adult brain show clear evidence of neurodegeneration (Lucas et al., 2001). Moreover, aberrantly activated GSK3β phosphorylates Tau, which leads to NFTs (Hanger et al., 1992). This evidence clearly indicated that GSK3β plays essential roles in the pathology of AD. Importantly, we and other groups previously reported that PS1, a causative molecule of familial AD, was also phosphorylated by GSK3β at serine 353, 357 residues (Kirschenbaum et al., 2001; Twomey and McCarthy, 2006; Uemura et al., 2007). Since most of the familial AD-linked PS1 mutations affect APP metabolism, in the present study, we examined the effect of PS1 phosphorylation on APP cleavage by PS1/γ-secretase. Our analysis using S353/357D mutant PS1 revealed that phosphorylated PS1 significantly inhibited the cleavage of APP CTFs by γ-secretase (Fig. 1A–D). Furthermore, the ELISA results indicated that PS1 phosphorylation reduced extracellular Aβ 40 levels without changing extracellular Aβ 42 levels, thereby increasing the Aβ 42/40 ratio (Fig. 1G–I). Similar phenomena were observed in the familial AD-linked PS1 mutations (Selkoe and Wolfe, 2007). Accumulating evidence suggests that partial loss of function in γ-secretase may lead to an increased Aβ 42/40 ratio as well as to neurodegeneration (Shen and Kelleher, 2007; Wolfe, 2007). In addition, a recent report suggested that Aβ 40 may inhibit Aβ deposition and thus may be physiologically neuroprotective (Kim et al., 2007).

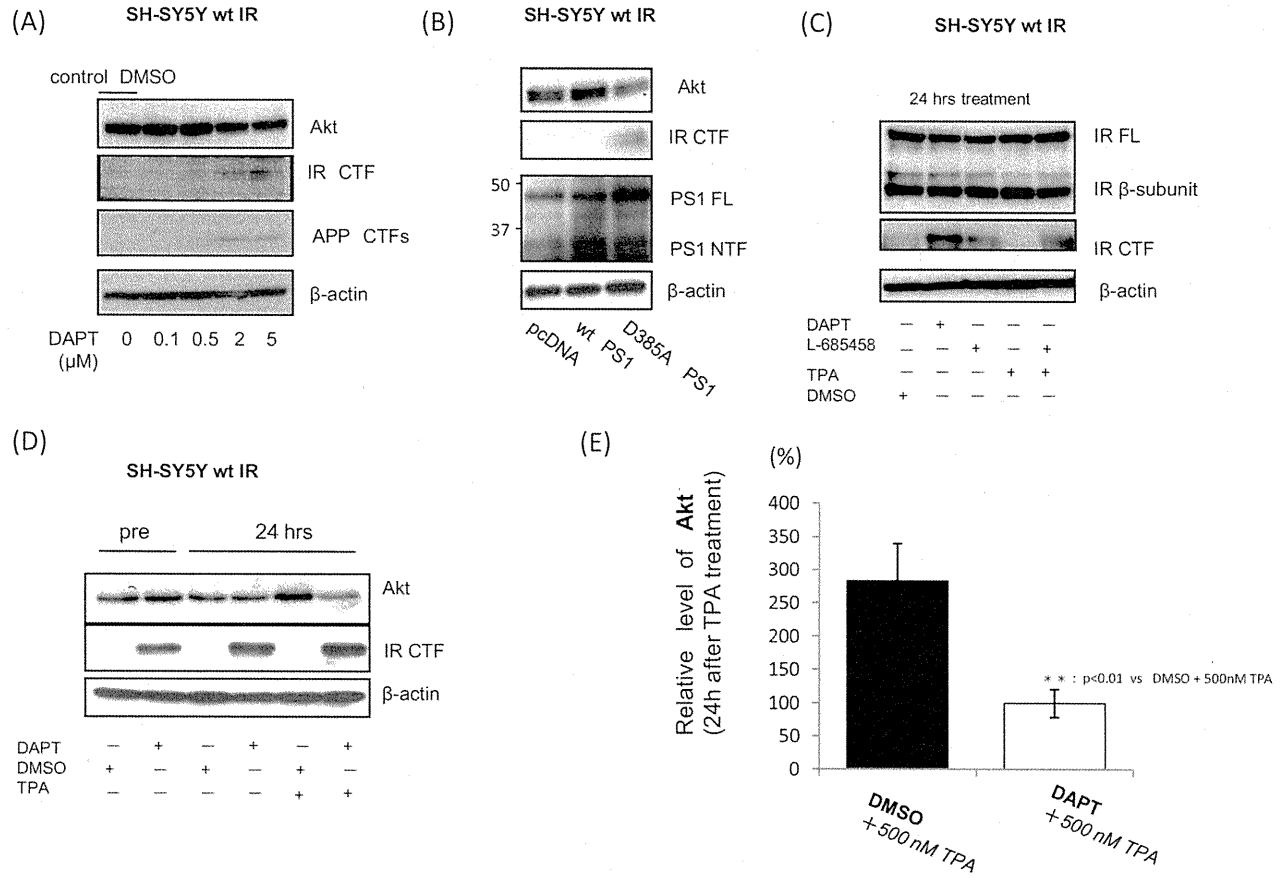

Fig. 5. IR cleavage changes the expression level of Akt. (A) SH-SY5Y wt IR cells were treated with DAPT for 24 h in different concentrations (0, 0.1, 0.5, 2, 5 μM). (B) SH-SY5Y wt IR cells were transiently transfected with pcDNA (as a control), wt PS1 and D385A PS1. After 48 h, the Akt level was analyzed. (C) SH-SY5Y wt IR cells were treated with 5 μM of DAPT, L-685458, 500 nM of TPA or L-685458+TPA for 24 h. Control cells were treated with DMSO. (D) After pre-incubation with either DAPT or vehicle (DMSO) for 18 h, SH-SY5Y wt IR cells were treated with 500 nM TPA in the presence of DAPT or DMSO for 24 h. (E) After TPA treatment, the relative expression level of Akt was quantitatively analyzed (n=4). The level of Akt was normalized by that of β-actin.

Thus, PS1 phosphorylation-mediated reduction of Aβ 40 and increase of Aβ 42/40 ratio can aggravate the pathology of AD (Fig. 6, left panel). So far, the significance of PS1 modification including phosphorylation has not yet been fully investigated in AD brains. Importantly, our *in vivo* study clearly showed accelerated PS1 phosphorylation in sporadic AD patient brains (Fig. 2). Considering these results, the disruption of the balance of PS1 phosphorylation may lead to neurodegeneration via aberrant GSK3β activity.

In addition, we searched for the mechanisms inhibiting PS1 phosphorylation. In the present study, we found a novel role of γ-secretase-mediated IR cleavage as a protective safeguard from aberrant GSK3β activity (Fig. 6, right panel). IR is widely distributed in the brain with particularly high concentrations in neurons, both in the cell bodies as well as in synapses (Werther et al., 1987; Marks et al., 1991). IR is a known substrate for γ-secretase and IR ICD translocates to the nucleus upon γ-secretase-mediated cleavage (Kasuga et al., 2007). In this report, we showed that IR ICD activates the transcription of Akt (Fig. 4), a key element in multiple biological processes including glucose metabolism, cell survival, cell growth, cell differentiation, and angiogenesis (Franke et al., 2003; Fayard et al., 2005; Song et al., 2005). Notably, we observed that PS1 phosphorylation promoted the γ-secretase-mediated cleavage of IR (Fig. 3). Thus, GSK3β activation may promote the phosphorylation of PS1 to enhance cleavage of IR, finally activating the transcription of Akt, which is a strong inhibitor of GSK3β activity. This phenomenon may constitute a negative feedback mechanism, which up-regulates Akt when GSK3β is aberrantly activated. Interestingly, this is contrary to the case of the cleavage of N-cadherin, since N-cadherin cleavage is down-regulated by the phosphorylation of PS1 (Uemura et al., 2007). Thus, the phosphorylation status of PS1 may explain in part the substrate specificity in various conditions.

CONCLUSION

We propose that GSK3β-mediated PS1 phosphorylation, acting as a link between GSK3β activity and Aβ generation, may play a pivotal role in AD pathogenesis under the influence of insulin signaling. As our study indicated that GSK3β-mediated phosphorylation of PS1 increases the Aβ 42/40 ratio, modulating GSK3β activity can be a good

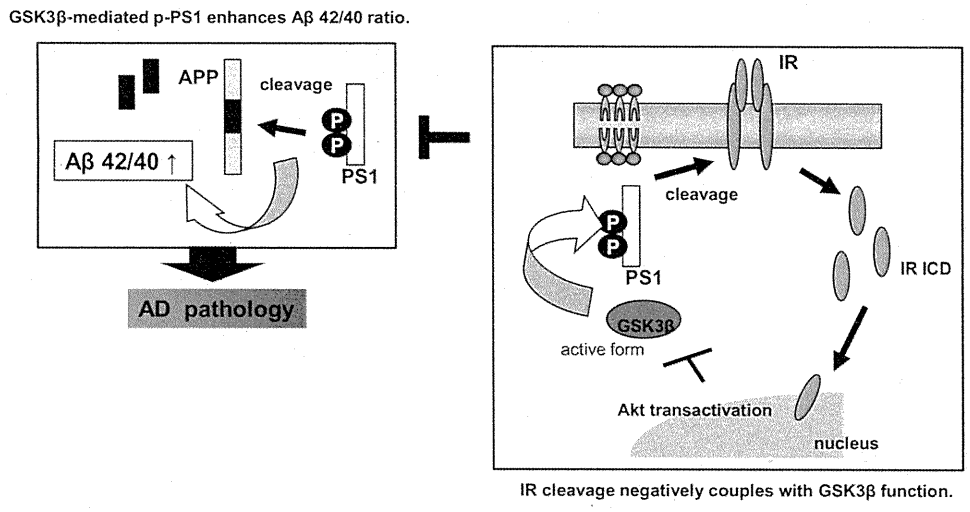

Fig. 6. Schematic presentation of cellular events caused by PS1 phosphorylation. GSK3β-mediated PS1 phosphorylation enhances the extracellular Aβ42/40 ratio and its phosphorylation is promoted in the AD brain. Therefore, PS1 phosphorylation may promote the pathology of AD (left panel). On the other hand, when GSK3β is aberrantly activated, the phosphorylated PS1 cleaves IR, then activates the transcription of Akt, which finally inhibits GSK3β activity (right panel). There may be some mechanisms which down-regulate PS1 phosphorylation through inhibition of GSK3β activity and IR cleavage by γ-secretase can be one of them.

therapeutic strategy, aiming at both the inhibition of tau phosphorylation and the reduction of Aβ 42/40 ratio. Thus, IR cleavage could be one of the potential regulatory mechanisms affecting GSK3β activity as a negative feedback mechanism; disruption of IR cleavage may lead to increased GSK3β activity, as well as Aβ 42/40 ratio. Therefore, the *in vivo* regulatory mechanism of controlling PS1 function including phosphorylation should be examined in future studies.

Acknowledgments—We greatly appreciate the gift of human Insulin Receptor (hIR) construct from Dr. T. Ikeuchi (Niigata University, Niigata, Japan), PS1/PS2 double knockout mouse embryonic fibroblast (MEF PS-/-) from Dr. B DeStrooper (Catholic University, Leuven, Belgium) and pcDNA3 with HA tag vector from Dr. R. Takahashi (Kyoto University, Kyoto, Japan). We would like to give our thanks to Dr. M. Kinoshita (Nagoya University, Nagoya, Japan) and Dr. A. Yanagida (Kyoto University, Kyoto, Japan) for technical assistance of Real-time PCR assay. We would like to give our thanks to Dr. S. Oka (Kyoto University, Kyoto, Japan), Mr. T. Kohno and Ms. N. Yamada for technical assistance of Tricine SDS-PAGE. The work was financially supported by Grant-in-Aid from the Ministry of Education, Culture, Sports, Science and Technology (20300124) and the Research Grant from Takeda Science Foundation.

REFERENCES

Bhat RV, Budd Haeberlein SL, Avila J (2004) Glycogen synthase kinase 3: a drug target for CNS therapies. J Neurochem 89: 1313–1317.

Braak H, Braak E (1991) Neuropathological stageing of Alzheimer-related changes. Acta Neuropathol 82:239–259.

Bradford MM (1976) A rapid and sensitive method for the quantitation of microgram quantities of protein utilizing the principle of protein-dye binding. Anal Biochem 72:248–254.

De Strooper B, Saftig P, Craessaerts K, Vanderstichele H, Guhde G, Annaert W, Von Figura K, Van Leuven F (1998) Deficiency of presenilin-1 inhibits the normal cleavage of amyloid precursor protein. Nature 391:387–390.

Ebina Y, Edery M, Ellis L, Standring D, Beaudoin J, Roth RA, Rutter WJ (1985) Expression of a functional human insulin receptor from a cloned cDNA in Chinese hamster ovary cells. Proc Natl Acad Sci U S A 82:8014–8018.

Fayard E, Tintignac LA, Baudry A, Hemmings BA (2005) Protein kinase B/Akt at a glance. J Cell Sci 118:5675–5678.

Francis R, McGrath G, Zhang J, et al. (2002) Aph-1 and pen-2 are required for Notch pathway signaling, gamma-secretase cleavage of betaAPP, and presenilin protein accumulation. Dev Cell 3:85–97.

Franke TF, Hornik CP, Segev L, Shostak GA, Sugimoto C (2003) PI3K/Akt and apoptosis: size matters. Oncogene 22:8983–8998.

Goutte C, Tsunozaki M, Hale VA, Priess JR (2002) APH-1 is a multipass membrane protein essential for the Notch signaling pathway in *Caenorhabditis elegans* embryos. Proc Natl Acad Sci U S A 99:775–779.

Grundke-Iqbal I, Iqbal K, Quinlan M, Tung YC, Zaidi MS, Wisniewski HM (1986) Microtubule-associated protein tau. A component of Alzheimer paired helical filaments. J Biol Chem 261:6084–6089.

Hanger DP, Hughes K, Woodgett JR, Brion JP, Anderton BH (1992) Glycogen synthase kinase-3 induces Alzheimer's disease-like phosphorylation of tau: generation of paired helical filament epitopes and neuronal localisation of the kinase. Neurosci Lett 147:58–62.

Kasuga K, Kaneko H, Nishizawa M, Onodera O, Ikeuchi T (2007) Generation of intracellular domain of insulin receptor tyrosine kinase by gamma-secretase. Biochem Biophys Res Commun 360: 90–96.

Kim J, Onstead L, Randle S, Price R, Smithson L, Zwizinski C, Dickson DW, Golde T, McGowan E (2007) Abeta40 inhibits amyloid deposition *in vivo*. J Neurosci 27:627–633.

Kirschenbaum F, Hsu SC, Cordell B, McCarthy JV (2001) Substitution of a glycogen synthase kinase-3beta phosphorylation site in presenilin 1 separates presenilin function from beta-catenin signaling. J Biol Chem 276:7366–7375.

Linda A, Sofia H, Gerd M, Kerstin I (2007) IGF-1-induced processing of the amyloid precursor protein family is mediated by different signaling pathways. J Biol Chem 282:10203–10209.

Lucas J, Hernández F, Gómez-Ramos P, Morán M, Hen R, Avila J (2001) Decreased nuclear beta-catenin, tau hyperphosphorylation and neurodegeneration in GSK-3beta conditional transgenic mice. EMBO J 20:27–39.

Maesako M, Uemura K, Kubota M, et al. (2010) Insulin regulates presenilin 1 localization via PI3k/Akt signaling. Neurosci Lett 483: 157–161.

Maetzel D, Denzel S, Mack B, et al. (2009) Nuclear signalling by tumour-associated antigen EpCAM. Nat Cell Biol 11:162–171.

Marambaud P, Shioi J, Serban G, et al. (2002) A presenilin-1/gamma-secretase cleavage releases the E-cadherin intracellular domain and regulates disassembly of adherens junctions. EMBO J 21: 1948–1956.

Marks JL, King MG, Baskin DG (1991) Localization of insulin and type 1 IGF receptors in rat brain by *in vitro* autoradiography and *in situ* hybridization. Adv Exp Med Biol 293:459–470.

Mirra SS, Heyman A, McKeel D, Sumi SM, Crain BJ, Brownlee LM, Vogel FS, Hughes JP, van Belle G, Berg L (1991) The Consortium to Establish a Registry for Alzheimer's disease (CERAD). Part II: standardization of the neuropathologic assessment of Alzheimer's disease. Neurology 41:479–486.

Ni CY, Murphy MP, Golde TE, Carpenter G (2001) Gamma-secretase cleavage and nuclear localization of ErbB-4 receptor tyrosine kinase. Science 294:2179–2181.

Okamoto I, Kawano Y, Murakami D, Sasayama T, Araki N, Miki T, Wong AJ, Saya H (2001) Proteolytic release of CD44 intracellular domain and its role in the CD44 signaling pathway. J Cell Biol 155:755–762.

Sastre M, Steiner H, Fuchs K, Capell A, Multhaup G, Condron MM, Teplow DB, Haass C (2001) Presenilin-dependent gamma-secretase processing of beta-amyloid precursor protein at a site corresponding to the S3 cleavage of notch. EMBO Rep 9:835–841.

Selkoe D, Wolfe MS (2007) Presenilin: running with scissors in the membrane. Cell 131:215–221.

Shen J, Kelleher RJ (2007) The presenilin hypothesis of Alzheimer's disease: evidence for a loss-of-function pathogenic mechanism. Proc Natl Acad Sci U S A 104:403–409.

Song G, Ouyang G, Bao S (2005) The activation of Akt/PKB signaling pathway and cell survival. J Cell Mol Med 9:59–71.

Steiner H, Capell A, Pesold B, Citron M, Kloetzel PM, Selkoe DJ, Romig H, Mendla K, Haass C (1998) Expression of Alzheimer's disease-associated presenilin-1 is controlled by proteolytic degradation and complex formation. J Biol Chem 273:32322–32331.

Twomey C, McCarthy JV (2006) Presenilin-1 is an unprimed glycogen synthase kinase-3beta substrate. FEBS Lett 580:4015–4020.

Uemura K, Kitagawa N, Kohno R, Kuzuya A, Kageyama T, Shibasaki H, Shimohama S (2003) Presenilin 1 mediates retinoic acid-induced differentiation of SH-SY5Y cells through facilitation of Wnt signaling. J Neurosci Res 73:166–175.

Uemura K, Kuzuya A, Shimozono Y, Aoyagi N, Ando K, Shimohama S, Kinoshita A (2007) GSK3beta activity modifies the localization and function of presenilin 1. J Biol Chem 282:15823–15832.

Uemura K, Lill CM, Banks M, et al. (2009) N-cadhrtin-based adhesion enhances Abeta release and decreases Abeta 42/40 ratio. J Neurochem 108:350–360.

Werther GA, Hogg A, Oldfield BJ, McKinley MJ, Figdor R, Allen AM, Mendelsohn FA (1987) Localization and characterization of insulin receptors in rat brain and pituitary gland using *in vitro* autoradiography and computerized densitometry. Endocrinology 121:1562–1570.

Wolfe MS (2007) When loss is gain: reduced presenilin proteolytic function leads to increased Abeta42/Abeta40. Talking point on the role of presenilin mutations in Alzheimer disease. EMBO Rep 8:136–140.

Wolfe MS, Kopan R (2004) Intramembrane proteolysis: theme and variations. Science 305:1119–1123.

Yu G, Nishimura M, Arawaka S, et al. (2000) Nicastrin modulates presenilin-mediated notch/glp-1 signal transduction and betaAPP processing. Nature 407:48–54.

(Accepted 14 December 2010)
(Available online 13 January 2011)

THE JOURNAL OF BIOLOGICAL CHEMISTRY VOL. 286, NO. 9, pp. 7619–7628, March 4, 2011

N-cadherin Regulates p38 MAPK Signaling via Association with JNK-associated Leucine Zipper Protein

IMPLICATIONS FOR NEURODEGENERATION IN ALZHEIMER DISEASE[S]

Received for publication, June 26, 2010, and in revised form, December 21, 2010 Published, JBC Papers in Press, December 22, 2010, DOI 10.1074/jbc.M110.158477

Koichi Ando[‡], Kengo Uemura[§], Akira Kuzuya[‡], Masato Maesako[¶], Megumi Asada-Utsugi[¶], Masakazu Kubota[¶], Nobuhisa Aoyagi[‡], Katsuji Yoshioka[‖], Katsuya Okawa[**], Haruhisa Inoue[‡‡], Jun Kawamata[‡], Shun Shimohama[§§], Tetsuaki Arai[¶¶], Ryosuke Takahashi[‡], and Ayae Kinoshita[¶1]

From the [¶]School of Human Health Sciences, Kyoto University Graduate School of Medicine, Kyoto 606-8507, Japan, the [‡]Department of Neurology, Kyoto University Graduate School of Medicine, Kyoto 606-8507, Japan, [§]Massachusetts General Hospital, Harvard Medical School, Charlestown, Massachusetts 02129, the [‖]Division of Molecular Cell Signaling, Cancer Research Institute, Kanazawa University, Kanazawa 920-1192, Japan, [**]Kyowa Hakko Kirin Co., Tokyo 100-8185, Japan, the [‡‡]Center for iPS Cell Research and Application, Kyoto University, Kyoto 606-8507, Japan, the [§§]Department of Neurology, Sapporo Medical University, Sapporo 060-8556, Japan, and the [¶¶]Tokyo Institute of Psychiatry, Tokyo 156-8585, Japan

Synaptic loss, which strongly correlates with the decline of cognitive function, is one of the pathological hallmarks of Alzheimer disease. N-cadherin is a cell adhesion molecule essential for synaptic contact and is involved in the intracellular signaling pathway at the synapse. Here we report that the functional disruption of N-cadherin-mediated cell contact activated p38 MAPK in murine primary neurons, followed by neuronal death. We further observed that treatment with $A\beta_{42}$ decreased cellular N-cadherin expression through NMDA receptors accompanied by increased phosphorylation of both p38 MAPK and Tau in murine primary neurons. Moreover, expression levels of phosphorylated p38 MAPK were negatively correlated with that of N-cadherin in human brains. Proteomic analysis of human brains identified a novel interaction between N-cadherin and JNK-associated leucine zipper protein (JLP), a scaffolding protein involved in the p38 MAPK signaling pathway. We demonstrated that N-cadherin expression had an inhibitory effect on JLP-mediated p38 MAPK signal activation by decreasing the interaction between JLP and p38 MAPK in COS7 cells. Also, this study demonstrated a novel physical and functional association between N-cadherin and p38 MAPK and suggested neuroprotective roles of cadherin-based synaptic contact. The dissociation of N-cadherin-mediated synaptic contact by Aβ may underlie the pathological basis of neurodegeneration such as neuronal death, synaptic loss, and Tau phosphorylation in Alzheimer disease brain.

Alzheimer disease (AD)[2] is pathologically characterized by the presence of amyloid β-peptide (Aβ) and neurofibrillary tangles in the neocortex and hippocampus. Insoluble Aβ fibrillar aggregates found in senile plaques have long been considered to cause the neurodegeneration of AD. On the other hand, synaptic loss is another pathological hallmark of AD, which strongly correlates with the severity of cognitive impairment better than senile plaques or neurofibrillary tangles (1). Interestingly, recent studies from AD mouse models have shown that learning impairment and synaptic dysfunction become apparent before the formation of plaques, suggesting the hypothesis that soluble Aβ causes "synaptic failure" before plaques develop and neuron death occurs (2). Converging lines of evidence suggest that natural soluble Aβ oligomers trigger synaptic loss (3). Thus, in addition to the investigation of molecular mechanisms, which develop senile plaques and neurofibrillary tangles, research focusing on synaptic dysfunction is important to clarify the earliest pathology in AD.

Presenilin (PS) 1/2 is the essential catalytic component of γ-secretase proteolytic complex (4, 5), which is responsible for the final cleavage of amyloid precursor protein to generate Aβ peptides. Mutations in PS1 have been known as the most common cause of autosomal dominant familial Alzheimer disease (6–8). Interestingly, PS1 binds to N-cadherin, which is an essential molecule for synaptic contact and is abundantly localized in hippocampal synapses (9). The cytoplasmic domain of cadherin associates with the actin cytoskeleton via β-catenin and regulates synaptic contact, synaptogenesis, and dendritic spine morphology (10, 11). In addition to the structural role as an adhesive molecule, N-cadherin plays important roles in intracellular signaling pathways such as β-catenin or Wnt signaling. Also, N-cadherin-based cell-cell adhesion activates PI3K/Akt cell survival signaling by recruiting PI3K into the N-cadherin adhesion complex (12). Further, PS1 facilitates this process by promoting cadherin/PI3K association (13). As a consequence, PS1/N-cadherin interaction at the synapse seems to be neuroprotective by facilitating the PI3K/Akt survival signaling. Recently, we demonstrated that N-cadherin promotes the cell surface expression of PS1/γ-secretase, thereby activating the PI3K/Akt/GSK3β signaling pathway (14) and that N-cadherin-mediated synaptic adhesion modulates Aβ secretion as well as $A\beta_{42/40}$ ratio via PS1/

[S] The on-line version of this article (available at http://www.jbc.org) contains supplemental Figs. S1–S5.

[1] To whom correspondence should be addressed: School of Human Health Sciences, Kyoto University Graduate School of Medicine, 53, Shogoin-kawahara-cho, Sakyo-ku, Kyoto 606-8507, Japan. Tel./Fax: 81-75-751-3969; E-mail: akinoshita@hs.med.kyoto-u.ac.jp.

[2] The abbreviations used are: AD, Alzheimer disease; Aβ, amyloid β; JLP, JNK-associated leucine zipper protein; PS, presenilin; MTT, 3-(4,5-dimethylthiazol-2-yl)-2,5-diphenyltetrazolium bromide; ANOVA, analysis of variance.

N-cadherin interactions (15). Therefore, it is plausible that N-cadherin functions not only as a synaptic adhesion molecule but also as a modulator of AD pathology by affecting Aβ production and PI3K/Akt signaling.

On the other hand, increased p38 MAPK activity is associated with the neuropathology of AD (16). For example, both p38 MAPK and its upstream kinase MKK6 are activated in AD brain tissue as demonstrated by immunohistochemistry (17, 18). Activation of the p38 MAPK signaling is also reported in an AD-relevant animal model (19). Moreover, a previous report demonstrated that Aβ employs synaptic depression to drive endocytosis of synaptic AMPA receptor by activating p38 MAPK (20). Among the MAPK family members, p38 MAPK is activated by numerous unique signals such as environmental stressors and toxins, cellular injury, growth factors, and inflammatory cytokine leading to various neuronal cell fates including apoptosis, differentiation, and proliferation. However, the relationship between p38 MAPK and N-cadherin has not been elucidated in AD pathology.

Based on the above observations, we hypothesized that disruption of N-cadherin-based cell-cell contact may up-regulate the p38 MAPK signaling, leading to the neurodegeneration of AD. We demonstrated an inverse correlation between the expression levels of phosphorylated (and thus activated) p38 MAPK and those of N-cadherin in human brains. Moreover, we showed that the disruption of N-cadherin-based contact leads to an activation of p38 MAPK signaling in murine primary neurons, followed by neuronal death. Furthermore, we performed proteomic analysis using human brains and identified JNK-associated leucine zipper protein (JLP) as a novel interacting protein of N-cadherin, thus demonstrating a new signaling pathway from N-cadherin to p38 MAPK through the association with JLP, which might be compromised in AD pathogenesis.

EXPERIMENTAL PROCEDURES

Human Material and Proteomics—Human brain tissues were provided by the Tokyo Institute of Psychiatry. Brains from non-AD and AD patients were dissolved in radioimmune precipitation assay buffer (50 mM Tris, pH 8.0, 1% Triton X-100, 0.1% SDS, 150 mM NaCl, 1% Nonidet P-40, and 0.5% deoxycholate) supplemented with protease inhibitor mixture (Roche Applied Science) and phosphatase inhibitor mixture (Sigma). Each sample was then centrifuged at 14,000 × *g* for 20 min at 4 °C, and the supernatants were collected to obtain soluble proteins. Protein concentration was determined using the Bradford assay. Equal amounts of protein were subjected to SDS-PAGE followed by Western blot. For proteomic analysis, equal amounts of aliquots were treated with protein G-Sepharose (GE Healthcare) for 1 h at 4 °C. After removing protein G-Sepharose by centrifugation at 2,000 × *g* for 5 min, anti-N-cadherin antibody (BD Biosciences) was added to the supernatants. Each sample was rotated for 2 h at 4 °C and then treated with protein G-Sepharose for 1 h at 4 °C. The immunoprecipitates were washed with radioimmune precipitation assay buffer five times and resuspended in 2× sample buffer (125 mM Tris-HCl, pH 6.8, 4.3% SDS, 30% glycerol, 10% 2-mercaptoethanol, and 0.01% bromphenol blue). After boiling for 4 min, the supernatants were subjected to SDS-PAGE. To visualize proteins, the gels were stained with silver nitrate using PlusOne silver staining kit protein (GE Healthcare). The protein bands were excised and subjected to in gel trypsinization, and molecular mass analysis of the tryptic peptides was performed by MALDI-TOF/MS with an Ultraflex MALDI-TOF/TOF system (Bruker Daltonics, Billerica, MA).

Cells, Plasmids, and Transfection—HEK293 and COS7 cells were maintained in DMEM (Sigma) containing 10% FBS (Invitrogen) and 1% penicillin/streptomycin at 37 °C in a 5% CO_2 incubator. SH-SY5Y cells, which are derived from human neuroblastoma cell lines, were maintained in Opti-MEM® (Invitrogen) containing 10% FBS. Primary neurons were obtained from the cerebral cortices of fetal mice (14–16 days of gestation) and cultured in neurobasal medium supplemented with B-27 (Invitrogen). Expression plasmids encoding S-tagged JLP and its mutant derivatives were kind gifts from Dr. Reddy (Temple University) (21). FLAG-tagged p38 MAPK and FLAG-tagged MKK4 (SEK1) were described previously (22). HA-tagged MEKK3 (Addgene plasmid 12186) was provided by Dr. Johnson (National Jewish Center for Immunology and Respiratory Medicine) (23). HA-tagged N-cadherin was described elsewhere (14). Transfection of either HEK293 or COS7 cells was carried out using Transfectin reagent (Bio-Rad) according to the manufacturer's protocol.

Antibodies and Reagents—The following antibodies were used in the study: mouse monoclonal antibody to N-cadherin (BD Biosciences), rabbit polyclonal antibody to JLP (Abcam), rabbit polyclonal antibody to p38 and phospho-p38 (Cell Signaling Technology), rabbit polyclonal antibody to S-probe (Santa Cruz Biotechnology), monoclonal and rabbit polyclonal anti-HA antibodies, mouse monoclonal anti-N-cadherin N terminus antibody (N-cadherin neutralizing antibody, GC-4), anti-β-actin antibody, anti-FLAG-M2 antibody, control normal mouse IgG (Sigma), mouse monoclonal antibody to PHF-Tau (AT8) (Pierce), and Alexa Fluor 546 goat anti-rabbit IgG conjugate and Alexa Fluor 488 goat anti-mouse IgG conjugate (Molecular Probe). ADH-1 was a kind gift from Dr. Gupta (Adherex Technologies Inc.). Synthetic $A\beta_{42}$ peptides were obtained from Peptide Institute Inc. SB203580 was purchased from Calbiochem. S-protein-agarose beads were from Novagen.

Western Blot, Immunoprecipitation, Pulldown Assay, MTT Assay, and Cell Treatment by Reagents—Preparation of protein samples, Western blot, and immunoprecipitation were carried out as described elsewhere (14). Pull-down assay using S-protein-agarose beads (Novagen) was carried out as described elsewhere (21). MTT assay was performed using the MTT cell proliferation assay kit (Cayman) according to the manufacturer's instructions. For inhibition of N-cadherin-mediated cell-cell contact, the cells were treated either with ADH-1 as indicated or with N-cadherin-neutralizing antibody (GC-4) as described elsewhere (15).

Immunostaining—The samples for immunostaining were prepared as described elsewhere (15). After fixation, the samples were examined using a laser scanning confocal microscope, LSM 510 META (Zeiss).

TABLE 1
Characteristics of human cases
Clinical and histopathological information on brain samples used for analysis in Fig. 1*A*. We analyzed five AD patient brains confirmed by neuropathology and five control subjects without neurological complications. There is no statistical difference in age between AD and control cases. NA, not available. NFT, neurofibrillary tangle.

Case	Age	Sex	Post-mortem interval	Clinical diagnosis	Pathological findings
	years		*h*		
Non-AD					
Case 1	60	Male	NA	Alcoholism	Plaque(−), NFT stage I
Case 2	80	Female	NA	Abdominal aortic aneurysm rupture	Plaque(−), NFT stage II
Case 3	77	Male	7.5	Liver cirrhosis	Plaque(−), NFT stage II
Case 4	66	Male	11	Rectal cancer	Plaque(−), NFT stage I
Case 5	48	Male	10	Familial idiopathic basal ganglia calcification	Plaque(−), tangle(−)
AD					
Case 1	75	Male	12	Alzheimer disease	Braak stage C, VI
Case 2	68	Female	9	Alzheimer disease	Braak stage C, VI
Case 3	75	Male	17.5	Alzheimer disease	Braak stage C, VI
Case 4	81	Female	61	Dementia with Levy bodies	Alzheimer disease Braak stage C, VI
Case 5	56	Male	18	Alzheimer disease	Braak stage C, VI

Statistical Analysis—Signals on films were quantified with National Institutes of Health Image software (National Institutes of Health). Comparisons were performed using a Mann-Whitney *U* test or a Student's *t* test. For comparison of multiparametric analysis, one-way ANOVA, followed by the post hoc analysis by Fisher's protected least significant difference (PLSD) was used. Pearson's correlation co-efficients and significance were defined by STATVIEW software. The data are expressed as the means ± S.E., and statistical significance was assessed at $p < 0.05$.

RESULTS

The Expression Levels of Phosphorylated p38 MAPK Were Negatively Correlated with N-cadherin Expression Levels in Human Brains—N-cadherin is an essential adhesion molecule for forming synapses, and synaptic loss is one of pathological hallmarks of AD. Because previous reports showed that synaptic proteins such as synaptophysin or PSD-95 were reduced in AD (24, 25), we hypothesized that N-cadherin expression is also decreased in the brains of AD patients. First, the expression levels of N-cadherin were analyzed in human brain tissues from temporal cortices of AD patients and age-matched non-AD controls (Table 1). As expected, Western blot analysis using anti-N-cadherin antibody showed that expression levels of N-cadherin were decreased in AD brains compared with non-AD controls (Fig. 1*A*). Quantitative analysis showed that the ratio of N-cadherin/β-actin was significantly decreased in AD brains compared with that in non-AD controls (Fig. 1*B*, $p < 0.05$). To investigate whether the phosphorylation of p38 MAPK was enhanced in AD brains, we subsequently examined the expression levels of both phosphorylated and total p38 MAPK in the same tissues of human brains by Western blot (Fig. 1*A*). Consistent with previous reports (18–20), quantitative analysis showed a significant increase in the ratio of phospho/total p38 MAPK in AD brains, compared with that in non-AD controls (Fig. 1*C*, $p < 0.01$). Moreover, when we plotted the ratio of phospho/total p38 MAPK against that of N-cadherin/β-actin, we found that the phospho/total p38 MAPK ratio negatively correlated with N-cadherin/β-actin ratio (Fig. 1*D*, $r = -0.774$, $p < 0.01$). These results suggested a negative correlation between phosphorylated p38 MAPK and N-cadherin expressions in human brain.

ADH-1 (N-cadherin Antagonist) Induced Neuronal Cell Death by Activating p38 MAPK in Murine Primary Neurons—To elucidate the link between the reduced level of N-cadherin and p38 MAPK activation in AD brains, we analyzed whether the inhibition of N-cadherin-based synaptic contact could lead to p38 MAPK activation in neuronal cells. The N-terminal extracellular domain of N-cadherin harbors the homophilic cell adhesion recognition sequence, His-Ala-Val (HAV). It has been established that ADH-1, which mimics the natural HAV sequence of N-cadherin, can specifically disrupt N-cadherin-mediated cell adhesion (26). Therefore, we used it as a specific N-cadherin antagonist in the present experiment. First, murine primary neurons were treated with different concentrations of ADH-1 to disrupt the N-cadherin-based synaptic contact, followed by analysis of p38 MAPK activation by Western blot. Interestingly, exposure of murine primary neurons to ADH-1 for 24 h enhanced the phosphorylation of p38 MAPK and Tau in a concentration-dependent manner (Fig. 2*A* and supplemental Fig. S1). To confirm the effect of N-cadherin inhibition on p38 MAPK signaling and Tau phosphorylation in an alternative way, we applied N-cadherin-neutralizing antibody to murine primary neurons for 6 h followed by Western blot, and the same result was obtained as ADH-1 (supplemental Fig. S2). Next, we asked whether activation of p38 MAPK after inhibition of N-cadherin-based synaptic contact could lead to neuronal death. To answer this question, we examined neuronal cell viability after ADH-1 treatment using MTT assay. We observed significant decreases in neuronal cell viability after treatment with ADH-1 ($n = 4$, $p < 0.001$) (Fig. 2*B*). To evaluate whether p38 MAPK plays an important role in ADH-1-induced neuronal death, we used SB203580, a well characterized p38 MAPK-specific inhibitor. ADH-1 application with or without SB203580 revealed that neuronal death induced by ADH-1 was significantly attenuated by co-treatment with SB203580 ($n = 4$, $p < 0.001$) (Fig. 2*C*). Thus, the increased level of p38 MAPK activation is responsible for the ADH-1-induced neuronal death. To prove the effect of ADH-1 on the structural integrity of N-cadherin-mediated cell contact and p38 MAPK activation, ADH-1 (0.5 mg/ml) was added to confluent SH-SY5Y cells for 24 h. As expected, confocal microscopic analysis showed that

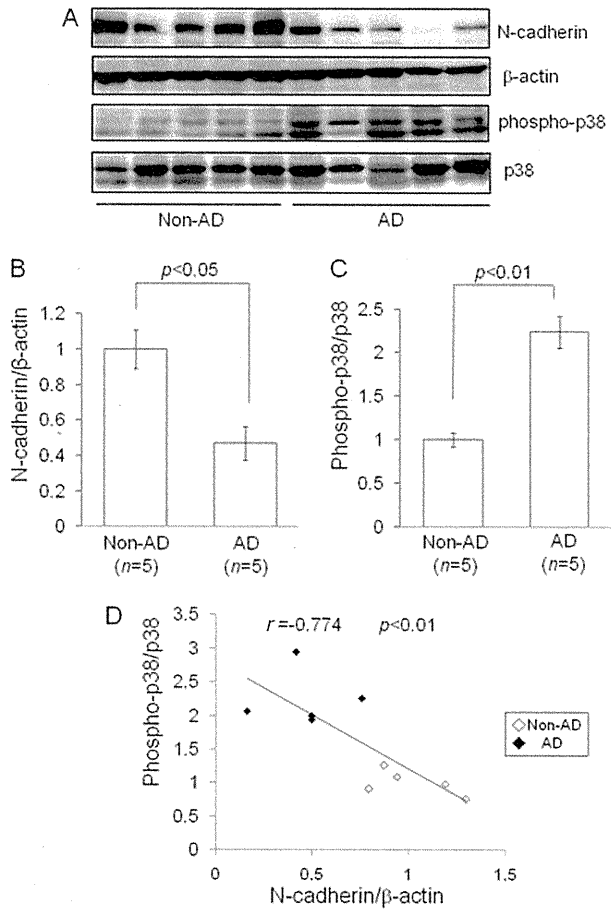

FIGURE 1. **Increased phospho-p38 MAPK expressions were negatively correlated with decreased N-cadherin expressions in human brains.** *A*, brain homogenates of temporal cortex from AD patients (*AD*, $n = 5$) and age-matched non-AD controls (*Non-AD*, $n = 5$) were analyzed by Western blot using anti-N-cadherin, β-actin, phospho-p38, and p38 MAPK antibodies. *B*, the band densities of N-cadherin and control β-actin were quantified by National Institutes of Health Image. The ratio of N-cadherin to β-actin (*N-cadherin/β-actin*) was calculated and analyzed by Mann-Whitney's *U* test. The N-cadherin/β-actin ratio was significantly decreased in the brains of AD patients compared with that of non-AD controls ($p < 0.05$). *C*, the band densities of phospho-p38 and p38 MAPK were quantified by National Institutes of Health Image. The phospho/total p38 MAPK ratio was calculated and analyzed by Mann-Whitney's *U* test. The phospho/total p38 MAPK ratio was significantly increased in the brains of AD patients compared with that of non-AD controls ($p < 0.01$). *D*, significant correlation was established in comparison between the phospho/total p38 MAPK ratio and the N-cadherin/β-actin ratio by Pearson's correlation co-efficients. The phospho/total p38 MAPK ratio was negatively correlated with the N-cadherin/β-actin ratio in human brain samples. ($r = -0.774$, $p < 0.01$).

the treatment with ADH-1 resulted in the significant decrease of N-cadherin immunoreactivity at the sites of cell-cell contact (Fig. 2*D*, *left panels*), indicating the disruption of N-cadherin-mediated cell contact. Consistent with the above result, enhanced immunoreactivity of phospho-p38 MAPK was observed in cells treated with ADH-1, compared with non-treated cells (Fig. 2*D*, *middle panels*). No immunoreactivities of both N-cadherin and phospho-p38 MAPK were observed in the absence of primary antibodies (supplemental Fig. S3).

$A\beta_{42}$ Decreased N-cadherin Expression through NMDA Receptors in Murine Primary Neurons—A number of recent studies have found that Aβ is synaptotoxic (20, 27). Therefore, we next examined whether Aβ could down-regulate N-cadherin expression in neurons. To assess the effect of Aβ on N-cadherin expressions, murine primary neurons were treated with synthetic $A\beta_{42}$ peptides (100 nM) for 48 h and subjected to Western blot. As shown in Fig. 3*A*, $A\beta_{42}$ treatment decreased N-cadherin expression in neurons. Previous reports have demonstrated that p38 MAPK is activated by the fibrillar Aβ (28) and that p38 MAPK can phosphorylate Tau at Ser-202/Thr-205 (29). Thus, we examined whether synthetic $A\beta_{42}$ peptides could trigger p38 MAPK activation and Tau phosphorylation at Ser-202/Thr-205 in our system. Consistent with the previous reports, we observed increased levels of phosphorylated p38 MAPK and phosphorylated Tau in the $A\beta_{42}$-treated cell preparations as compared with nontreated ones by Western blot ($n = 3$, $p < 0.01$) (Fig. 3, *A* and *B*). Together, this experiment indicated that $A\beta_{42}$ treatment decreases the levels of N-cadherin, activates p38 MAPK, and phosphorylates Tau in neuronal cells. Previous reports demonstrated that Aβ treatment induces excessive excitation of glutamate receptors to cause excitotoxicity (30, 31). Thus, we hypothesized that the decreased level of N-cadherin was induced by the Aβ-mediated excitotoxicity. To test this, murine primary neurons were pretreated (30 min) with the NMDA receptor antagonist MK-801 (10 μM) before being exposed to $A\beta_{42}$. Subsequent Western blot analysis of cell lysates revealed that MK-801 inhibited $A\beta_{42}$-induced reduction of N-cadherin levels ($n = 3$, $p < 0.05$) (Fig. 3*C*).

N-cadherin Associates with JLP Both in Human Brains and in Murine Primary Neurons—To clarify the mechanistic link between the disruption of N-cadherin-based contact and p38 MAPK activation, we set out to identify the proteins that associate with N-cadherin in human brain samples. For this, lysates of temporal cortices from brains of AD and non-AD patients were immunoprecipitated with anti-N-cadherin antibody, and the immunoprecipitates were subsequently subjected to SDS-PAGE. The separated proteins were visualized by silver staining, demonstrating a protein band of ~180 kDa in the lysates of brains of both AD patients and non-AD controls (supplemental Fig. S4). The protein band was identified by mass spectrometry as JLP, a scaffold protein that has been known to mediate the interaction between p38 MAPK and its upstream kinases (21). To confirm the association between N-cadherin and JLP, we transiently transfected HA-tagged N-cadherin and/or FLAG-tagged JLP expression constructs into HEK293 cells. Equal amounts of cell lysates obtained from each transfected cell were immunoprecipitated with anti-HA antibody and then immunoblotted with anti-FLAG antibody (Fig. 4*A*). A protein band of ~180 kDa was visualized with anti-FLAG antibody in the immunoprecipitate using anti-HA antibody obtained from the double-transfected cells (Fig. 4*A*, *third lane*), clearly indicating that N-cadherin associates with JLP. To further verify this association, the lysates derived from HEK293 cells transiently transfected with HA-tagged N-cadherin and/or FLAG-tagged JLP plasmids were immunoprecipitated with anti-FLAG antibody. As shown in Fig. 4*B*, HA-tagged immunoreactivity was observed in the immunoprecipitate with anti-FLAG antibody, confirming the association of N-cadherin with JLP. Finally, to demonstrate the endogenous association between N-cadherin and JLP in

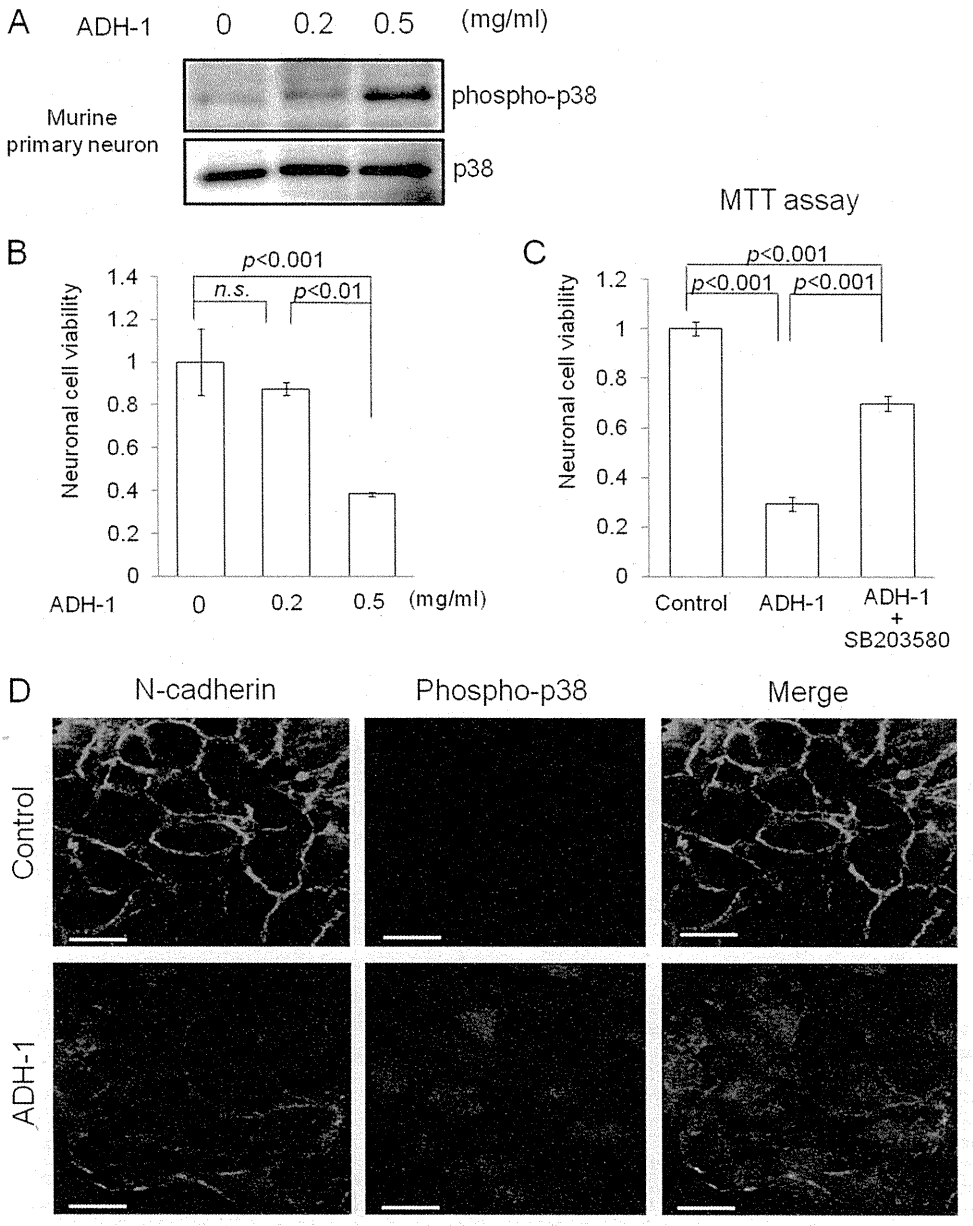

FIGURE 2. **ADH-1 induced neuronal cell death by activating p38 MAPK in murine primary neurons.** *A*, ADH-1, N-cadherin antagonist, was applied to murine primary neurons at different concentrations as shown. 24 h after treatment, the lysates were immunoblotted with anti-phospho-p38 and p38 MAPK antibodies. ADH-1 increased phosphorylation of p38 MAPK. *B*, neuronal cell death induced by ADH-1 was evaluated by MTT assay ($n = 5$, $p < 0.001$). *C*, murine primary neurons were treated with ADH-1 (0.5 mg/ml) for 24 h with or without 30 min of pretreatment with 10 μM SB203580, a specific p38 MAPK inhibitor, and the cell death was examined by MTT assay ($n = 4$, $p < 0.001$). SB203580 attenuated neuronal cell death induced by ADH-1 ($n = 4$, $p < 0.001$). *D*, ADH-1 (0.5 mg/ml) was added to confluent SH-SY5Y cells for 24 h followed by the immunostaining, using anti-N-cadherin and anti-phospho-p38 antibodies. Treatment with ADH-1 perturbed N-cadherin immunoreactivity, indicating a partial loss of N-cadherin from cell-cell junctions. *Scale bar*, 10 μm.

neurons, murine primary neurons were lysed, immunoprecipitated with anti-N-cadherin antibody, and then subjected to Western blot with anti-JLP antibody (Fig. 4*C*). The result showed endogenous association between N-cadherin and JLP in murine primary neurons, as well as in human brains.

N-cadherin/JLP Association Is Mediated by the Region Spanning Amino Acids 160–209 and Leucine Zipper II Domain of JLP—To determine the N-cadherin-binding domains of JLP, a series of S-tagged JLP mutants truncated at the C terminus was transfected into COS7 cells (Fig. 5*A*). Immunoprecipitation with anti-N-cadherin antibody showed that all of the S-tagged C-terminal deletion mutants of JLP were associated with N-cadherin (Fig. 5*B*), indicating that the JLP N terminus plays an important role in the association with N-cadherin. To further characterize the sequences of JLP involved in this association, various N-terminally truncated JLP mutants tagged with the S-sequence were prepared as indicated (Fig. 5*C*). COS7 cells were transiently transfected with these deletion mutants, and the lysate derived from each transfected cell was subjected to immunoprecipitation assay with anti-N-cadherin antibody. We observed that the JLP fragment corresponding to the region of amino acids 160-463 was strongly associated with N-cadherin, whereas that corresponding to the region of amino acids 160–398 showed a weaker association with N-cadherin (Fig. 5*D*). In contrast, a shorter fragment corresponding to the region of amino